





# Heat stress reveals a specialized variant of the pachytene checkpoint in meiosis of *Arabidopsis thaliana*

Joke De Jaeger-Braet <sup>1</sup>, Linda Krause <sup>2</sup>, Anika Buchholz <sup>2</sup> and Arp Schnittger <sup>1,\*†</sup>

<sup>1</sup> Department of Developmental Biology, Institute of Plant Science and Microbiology, University of Hamburg, Hamburg, Germany

<sup>2</sup> Institute of Medical Biometry and Epidemiology, University Medical Center Hamburg-Eppendorf, Hamburg, Germany

\*Author for correspondence: arp.schnittger@uni-hamburg.de

†Senior author

J.D.J.B. and A.S. designed the research; J.D.J.B. performed the experiments; L.K. and A.B. performed the statistical analysis; J.D.J.B., L.K., A.B., and A.S. analyzed and discussed the data; J.D.J.B. and A.S. wrote the article; J.D.J.B., L.K., A.B., and A.S. revised and approved the article.

The author responsible for distribution of materials integral to the findings presented in this article in accordance with the policy described in the Instructions for Authors (<https://academic.oup.com/plcell>) is: Arp Schnittger (arp.schnittger@uni-hamburg.de).

## Abstract

Plant growth and fertility strongly depend on environmental conditions such as temperature. Remarkably, temperature also influences meiotic recombination and thus, the current climate change will affect the genetic make-up of plants. To better understand the effects of temperature on meiosis, we followed male meiocytes in *Arabidopsis thaliana* by live cell imaging under three temperature regimes: at 21°C; at heat shock conditions of 30°C and 34°C; after an acclimatization phase of 1 week at 30°C. This work led to a cytological framework of meiotic progression at elevated temperature. We determined that an increase from 21°C to 30°C speeds up meiosis with specific phases being more amenable to heat than others. An acclimatization phase often moderated this effect. A sudden increase to 34°C promoted a faster progression of early prophase compared to 21°C. However, the phase in which cross-overs mature was prolonged at 34°C. Since mutants involved in the recombination pathway largely did not show the extension of this phase at 34°C, we conclude that the delay is recombination-dependent. Further analysis also revealed the involvement of the ATAXIA TELANGIECTASIA MUTATED kinase in this prolongation, indicating the existence of a pachytene checkpoint in plants, yet in a specialized form.

## Introduction

Ambient temperature is one of the key environmental parameters that determines plant growth and fertility and has been the focal interest of many plant researchers. Understanding plant responses to temperature is further boosted by the ongoing climate change (Couteau et al., 1999; Collins, 2014; Anderson et al., 2016), during which crops are expected to be exposed to very high temperatures in the near future, threatening to sharply reduce crop yield (Hatfield and Prueger, 2015; Yue et al., 2019). For example, a

drop in yield of up to 22% for maize (*Zea mays*) can be observed with a 1°C increase in temperature (Kukul and Irmak, 2018). To counteract these detrimental effects and adjust breeding programs, it is vital to understand the changes imposed by temperature stress on yield-related traits at the cellular and molecular levels.

Central for sexual reproduction and fertility is meiosis; previous work has demonstrated its sensitivity to changes in environmental conditions, especially temperature (Bomblies et al., 2015; Morgan et al., 2017). Meiosis is a specialized cell

## IN A NUTSHELL

**Background:** One of the hidden, yet far-reaching consequences of the current climate change crisis is an alteration of how particular plant genetic characteristics are transmitted from parents to their offspring. The underlying reason fueling this genetic effects is that a key mechanism by which the offspring genotype is different from that of their parents, called meiotic recombination, is highly temperature-sensitive. Meiotic recombination takes place in specialized cells, called meiocytes, and is very important for sexual reproduction as the meiocytes produce cells that eventually form the gametes. Meiotic recombination is also central to agriculture, since this is the major route by which favorable features such as large grain size and efficient water use are combined in crops.

**Question:** Despite its importance, very little is known about how temperature affects recombination at the molecular level. Moreover, most studies of meiotic recombination in plants rely on fixed flower material and hence, the dynamic nature of meiotic recombination either cannot be or is not easily analyzed. To complement and expand on these studies, we followed meiocytes by live cell imaging in a flowering plant commonly used in molecular plant research, *Arabidopsis*.

**Findings:** Our work led to a detailed understanding of how temperature affects meiocytes and the progression of meiotic recombination. Importantly, we identified a previously unrecognized control mechanism for how plants react to temperature-induced failures in meiotic recombination.

**Next steps:** We would like to understand the nature of these failures during meiotic recombination in response to high temperatures and how they can be recognized by plants to be corrected, if possible.

division during which DNA replication is followed by two rounds of chromosome segregation (meiosis I and meiosis II), resulting in the reduction of DNA content by half as a prerequisite for a subsequent fusion between gametes and restoration of full genome size. Furthermore, meiosis I plays an important role for the generation of genetic diversity via cross-over (CO) formation during prophase I and the resulting new assortment of chromosome sets. COs are not only important for the generation of new allelic combinations but also ensure physical connections between homologous chromosomes (homologs) that are needed for their balanced segregation. COs become visible as chiasmata, which connect two homologs in the form of a bivalent at the end of prophase I.

The control and execution of meiotic recombination are highly conserved and as in other eukaryotes, meiotic recombination in plants is initiated by the conserved topoisomerase-like protein SPORULATION 11-1 (SPO11-1), which together with associated proteins catalyzes DNA double-stranded breaks (DSBs) in early meiosis (Keeney et al., 1997; Grelon et al., 2001; Stacey et al., 2006; Hartung et al., 2007). Subsequently, DSBs are processed by the MRN protein complex, comprising MEIOTIC RECOMBINATION 11 (MRE11), RADIATION 50 (RAD50), and NIJMEGEN BREAKAGE SYNDROME 1 (NBS1), and are subsequently recognized by the recombinases DISRUPTED MEIOTIC cDNA 1 (DMC1; Bishop et al., 1992; Couteau et al., 1999) and the RecA homolog RAD51 (Jachymczyk et al., 1981; Li et al., 2004). These recombinases mediate the invasion of the processed single-stranded DNA into the DNA double strand of the homolog. In the absence of DMC1, DSBs are repaired by inter-sister recombination, resulting in the absence of COs and, hence, causing the formation of unconnected homologs, called univalents. In *rad51* mutants, DSBs are not repaired, resulting in

severely fragmented chromosomes and complete sterility of the mutant plants.

Toward the end of prophase I, all DSBs are repaired, leading to either non-COs or COs. COs fall in one of the two classes: type I COs rely on the ZMM proteins (acronym from the budding yeast [*Saccharomyces cerevisiae*] Zip, Mer, and Msh proteins), including MUTS HOMOLOG 4 (MSH4), and are formed at a distance from each other due to CO interference (Su and Modrich, 1986; Higgins et al., 2004). Type II COs are catalyzed by a different set of proteins, including METHYL METHANESULFONATE SENSITIVITY AND UV SENSITIVE 81, and are not subjected to interference (Interthal and Heyer, 2000; Berchowitz et al., 2007).

Homologs remain connected to each other until cohesin, a proteinaceous ring that embraces the sister chromatids from each homolog, is opened by cleavage of its alpha kleisin subunit, RECOMBINANT PROTEIN 8 (REC8), along the chromosome arms in anaphase I, paving the road for the separation of the homologs, each to opposite cell poles and, hence, completing meiosis I (Cai et al., 2003; Brar et al., 2006).

The successful execution of meiotic recombination as means to equally segregate homologs and ensure genetic diversity is controlled by the pachytene checkpoint, or meiotic recombination checkpoint, in animals and yeast (Roeder and Bailis, 2000). This checkpoint delays meiotic progression until recombination defects are resolved. Consequently, several mutants, especially in the recombination pathway, for example, *dmc1* mutants, trigger this checkpoint, resulting in a prolonged arrest that can even lead to apoptosis in several species, including mouse (*Mus musculus*) (Bishop et al., 1992; Rockmill et al., 1995; Barchi et al., 2005; Lange et al., 2011).

A master regulator of the pachytene checkpoint is ATAXIA TELANGIECTASIA MUTATED (ATM), a kinase

activated by DNA damage, which triggers checkpoint signaling, promotes DSB repair, and also controls the number of DSBs by regulating SPO11-1 activity via a negative feedback loop (Lange et al., 2011). While ATM is present in plants and fulfills several important functions during meiosis, it was thought so far that a pachytene checkpoint did not exist in plants since mutants like *dmc1* do not arrest at pachytene and instead complete meiosis, leading to aneuploid gametes (Couteau et al., 1999; Grelon et al., 2001; Caryl et al., 2003; Higgins et al., 2004; Li et al., 2004, 2009b; Jones and Franklin, 2008).

Meiosis and in particular meiotic recombination are highly sensitive to environmental conditions, leading to meiotic failure in many different organisms, such as the nematode *Caenorhabditis elegans* (Bilgir et al., 2013), mice (Nebel and Hackett, 1961), wheat (*Triticum aestivum*; Pao and Li, 1948), and rose (*Rosa hybrida*; Pecrix et al., 2011). Elevated temperatures also affect the meiotic microtubule (MT) cytoskeleton, resulting in irregular spindle orientation, aberrant cytokinesis, and the production of unreduced gametes, polyads, and micronuclei in poplar (*Populus pseudo-simonii*), rose, and Arabidopsis (*Arabidopsis thaliana*; Pecrix et al., 2011; Wang et al., 2017; De Storme and Geelen, 2020; Hedhly et al., 2020).

Furthermore, while DSB numbers are reported to be unaffected at elevated temperatures in several organisms, for example, yeast and Arabidopsis (Modliszewski et al., 2018; Brown et al., 2020), other aspects of the recombination pathway were found to be altered by temperature, leading to diverse effects that differ depending on the environmental conditions and species. Chiasma frequency was shown to be highly sensitive to environmental conditions. At high temperatures, chiasma frequency decreases in some species, such as in spiderwort (*Tradescantia bracteata*), perfoliate bellwort (*Uvularia perfoliate*), wild garlic (*Allium ursinum*), and during female meiosis in barley (*Hordeum vulgare*; Dowrick, 1957; Loidl, 1989; Phillips et al., 2015; Lloyd et al., 2018; Modliszewski et al., 2018), while it increases in other species, for instance in barley (male meiosis), Arabidopsis, and the fungus *Sordaria fimicola* (Lamb, 1969; Phillips et al., 2015; Lloyd et al., 2018; Modliszewski et al., 2018). In Arabidopsis, the increase in CO frequency at high temperatures was shown to be due to elevated numbers of type I COs (Lloyd et al., 2018; Modliszewski et al., 2018). In addition, CO distribution is also altered by heat stress (Dowrick, 1957; Higgins et al., 2012). In barley (male meiosis), high temperatures (30°C) cause an increase in chiasmata at the interstitial/proximal region of chromosomes but an overall decrease in chiasmata per cell (Higgins et al., 2012). At very high temperatures (35°C and above), in many species, such as wheat, barley, and wild garlic, synapsis of the homologs fails, resulting in the formation of univalents (Pao and Li, 1948; Loidl, 1989; Higgins et al., 2012).

To obtain further insights into the effects of temperature on meiosis, we followed Arabidopsis male meiocytes under three different temperature regimes via live cell imaging

using a recently established setup (Prusicki et al., 2019). We obtained here a detailed picture of meiotic progression under heat stress. While meiocytes progressed through meiosis much faster at higher temperatures than at 21°C in general, a key discovery was that the length of pachytene/diakinesis is prolonged at 34°C. We did not observe an extension of pachytene/diakinesis when recombination was abolished. Since this extension was also eradicated in *atm* mutants, we conclude that Arabidopsis and likely other plants have a specialized form of the pachytene checkpoint that is only triggered by recombination intermediates, but not by the complete absence of recombination as is the case in other species.

## Results

### A cytological sensor of heat stress in meiocytes

To analyze the effects of increased temperatures on meiosis, we applied three different heat conditions reflecting possible environmental stress scenarios and matching conditions used in previous studies. Arabidopsis is typically grown between 18°C and 24°C, with our standard growth conditions being 21°C during the day and 18°C during the night (hereafter called 21°C). As a first stress condition, we used a heat shock of 30°C (HS30°C) and analyzed the effects on meiosis immediately. In parallel, we allowed plants to acclimatize to 30°C (during both day and night) in highly controlled growth chambers for 1 week (long-term, LT30°C) before analyzing meiosis. The third condition consisted of an even more severe heat stress of 34°C (HS34°C) that was also applied immediately and analyzed.

However, the proper and reliable application of heat stress to multicellular structures, such as anthers, can be challenging when the focus is on particular cells, like meiocytes, which are surrounded by many different cell layers, such as the tapetum layer and the epidermis. The multicellular environment and the size of these structures have the capacity to buffer temperatures, hence making it difficult to exactly time the moment when the heat stress will reach the cells of interest. To resolve this problem, we took advantage of the observation that stress granules (SGs) form at elevated temperatures in different plant tissues, for example, roots, leaves, and hypocotyls (Hamada et al., 2018; Modliszewski et al., 2018; Kosmacz et al., 2019; Chodasiewicz et al., 2020; Dubiel et al., 2020). These SGs were previously shown in Arabidopsis seedlings to contain the cell cycle regulator CYCLIN-DEPENDENT KINASE A;1 (CDKA;1; Kosmacz et al., 2019). CDKA;1 is a major regulator of meiotic progression as well as recombination and its encoding gene is highly expressed in Arabidopsis male meiocytes (Dissmeyer et al., 2007; Bulankova et al., 2010; Zhao et al., 2017, 2012; Wijnker et al., 2019; Sofroni et al., 2020; Yang et al., 2020). To test whether CDKA;1 might change its homogeneous cytosolic and nuclear localization pattern during meiosis upon heat stress, we applied the different temperature regimes to male meiocytes from plants carrying the *CDKA;1-mVenus* and the *TagRFP-TUA5* (encoding a fusion protein between the red



fluorescent protein [RFP] and TUBULIN ALPHA-5 [TUA5]) reporters, and followed the localization pattern of CDKA;1:mVenus during meiosis (Sofroni et al., 2020).

Under our standard Arabidopsis growth conditions (21°C) and in agreement with previous analyses, CDKA;1-mVenus uniformly localized to both the cytoplasm and the nucleus.

This localization shifted from preferentially cytosolic to predominantly nuclear in late leptotene to early pachytene, followed by an increased cytosolic accumulation in pachytene and diakinesis. After anaphases I and II, CDKA;1-mVenus accumulated again in the reforming nuclei (Yang et al., 2020; Figure 1A).

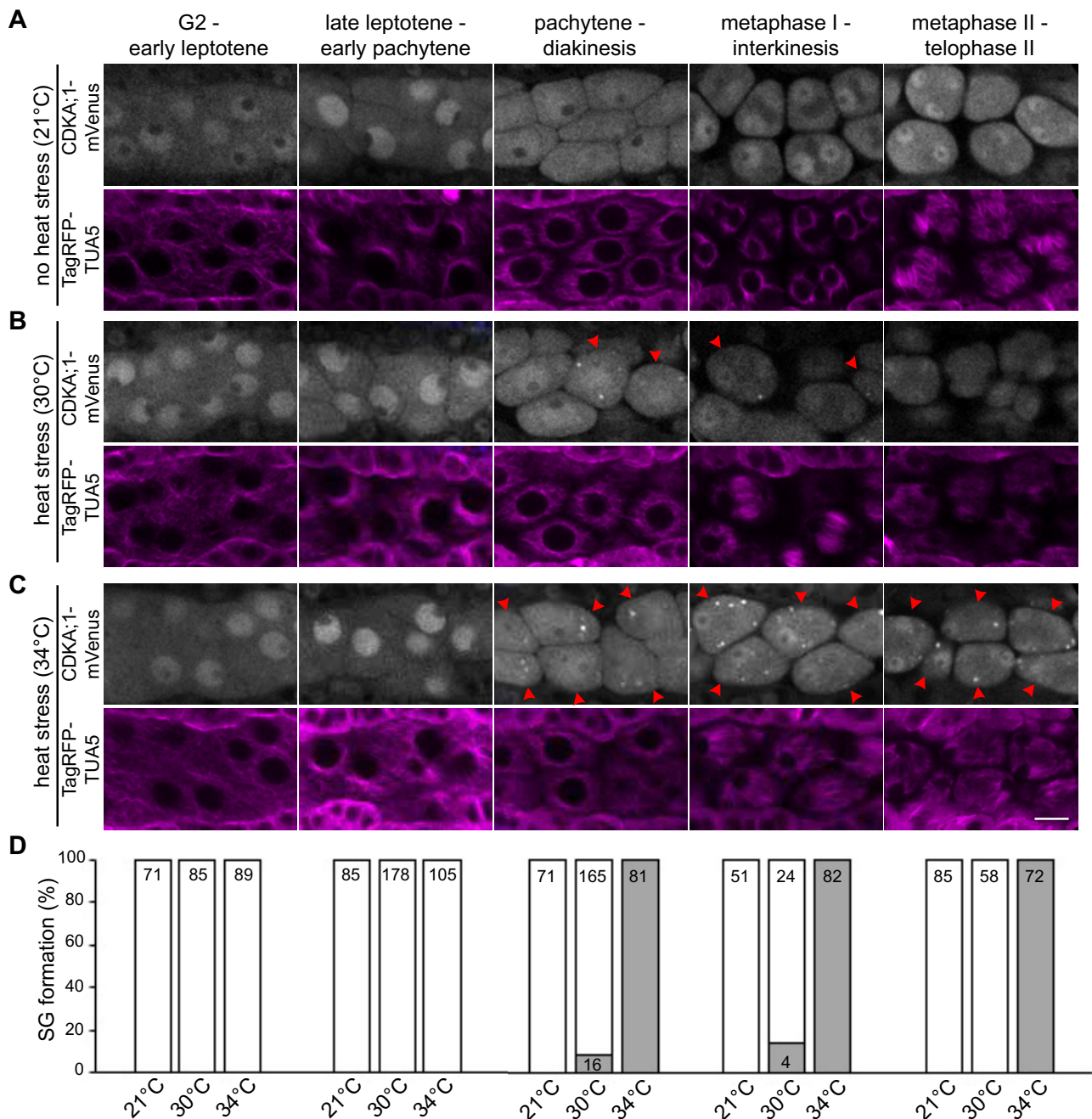


**Figure 1** Localization of CDKA;1 in male meiocytes under control and stress conditions. A–C, CDKA;1-mVenus (first row; white) and TagRFP-TUA5 (second row; magenta) localization under the control conditions of 21°C (A), heat stress of 30°C (B), or 34°C (C) at different meiotic stages: G2-early leptotene (Column 1), late leptotene-early pachytene (Column 2), pachytene-diakinesis (Column 3), metaphase I-interkinesis (Column 4), and metaphase II-telophase II (Column 5). Red arrowheads highlight cells with CDKA;1 localization at SGs. Scale bar, 10 µm. D, Quantification of CDKA;1 SG formation on the cellular level per stage in percent; white bar, cells without SGs; gray bar, cells with at least one SG. The absolute sample size is given in the corresponding bar.



At the elevated temperatures HS30°C and HS34°C, we observed the same cytosolic-nuclear localization dynamics for CDKA;1 (Figure 1, B and C). At HS34°C, we detected no SGs in early meiotic stages ( $n = 0/89$  in G2-early leptotene;  $n = 0/105$  from late leptotene to early pachytene), when CDKA;1 preferentially localized to the nucleus of meiocytes (Figure 1, C and D). Notably, SGs readily formed at HS34°C in all meiocytes from pachytene to diakinesis ( $n = 81/81$ ), from metaphase I to interkinesis ( $n = 82/82$ ), and from metaphase II to telophase II ( $n = 72/72$ ), that is the period when CDKA;1 starts to locate predominantly to the cytoplasm. These granules were visible about 15 min after the heat stress was applied, which was also the time required to set up the acquisition for live cell imaging at the microscope. Thus, the formation of SGs occurred within the first 15 min of heat stress.

In contrast, CDKA;1 granules rarely formed at HS30°C, that is in only 9% and 14% of the meiocytes in pachytene/diakinesis ( $n = 16/165$ ) and from metaphase I to interkinesis ( $n = 4/24$ ), respectively (Figure 1, B and D). In addition, the number of SGs per meiocyte was also lower at HS30°C compared to granule-containing meiocytes at HS34°C. These findings are consistent with the previous observation that the temperature threshold for the formation of SGs is around 34°C (Hamada et al., 2018).

Taken together, monitoring the formation of SGs allows the visualization of temperature stress in the tissue of interest. Importantly, this optical marker indicated that the ambient temperature reaches meiocytes in a short time, that is <15 min, paving the road for the faithful application of different heat treatments and their comparisons by live cell imaging.

### Heat stress affects MT configurations during meiosis in a quantitative but not qualitative manner

After having confirmed that the applied temperature regime reached male meiocytes fast and faithfully, we turned to addressing the general aim of this study, that is, how increased temperature affects the dynamics of meiosis. To tackle this question, we used a previously established live cell imaging method for meiosis (Prusicki et al., 2019). A crucial finding of this approach was the observation that meiosis can be dissected by the so-called landmarks that occur in a predictable order and that reflect highly defined cytological stages, for instance using fluorescently labeled MTs (TagRFP-TUA5). Thus, these landmarks not only allow the staging of meiocytes but also provide means to reveal the dynamics of meiosis by determining the time between landmarks.

In brief, MTs have the following dynamics during male meiosis: during G2-early leptotene, MTs are first homogeneously distributed in meiocytes with the nucleus in the center, for what is called MT array state 1 (Supplemental Figure S1A). MTs then will gradually polarize into a half moon-like structure on one side of the nucleus, which

defines MT array state 2-3-4, from late leptotene to early pachytene (Figure 2A; Supplemental Figure S1B). This structure develops further into a full moon-like assembly entirely surrounding the nucleus, marking MT array state 5-6, during pachytene, diplotene, and diakinesis (Figure 2B; Supplemental Figure S1C). After nuclear envelope breakdown (NEB), the prespindle transforms into the first meiotic spindle at MT array state 7-8-9, from metaphase I to anaphase I (Figure 2C; Supplemental Figure S1D). Next, MTs reorganize around the two newly formed nuclei and central MTs form a phragmoplast-like structure for MT array state 10-11 at telophase I and interkinesis (Figure 2D; Supplemental Figure S1E). The second division is characterized by the formation of two prespindles, followed by two spindles, at MT array state 12-13, from metaphase II to anaphase II (Figure 2E; Supplemental Figure S1F). Phragmoplast-like structures, which appear at MT array state 14, are visible at telophase II (Figure 2F; Supplemental Figure S1G) until cytokinesis, resulting in tetrads, the four meiotic products.

By analyzing meiosis at HS30°C, HS34°C, and LT30°C, we confirmed that meiosis does not arrest upon exposure to these temperature regimes, consistent with previous studies (De Storme and Geelen, 2020; Lei et al., 2020). Importantly, in all movies taken at higher temperatures (46 in total), the meiocytes progressed through the same MT array states as previously seen at 21°C (Movies 1–4; Supplemental Figure S1; Prusicki et al., 2019).

MT stability and polymerization are known to be temperature-sensitive (Bannigan et al., 2007; Li et al., 2009a; Wu et al., 2010; Liu et al., 2017; Song et al., 2020). Consistently, we observed quantitative changes in some MT structures, confirming that meiocytes were exposed to elevated temperatures. As revealed by pixel intensity quantification of meiocytes in MT array state 6, in which MTs fully surround the nucleus (Figure 3, A–D), we determined that the intensity of the fluorescence signal measured for TagRFP-TUA5 drops upon both HS30°C (Figure 3B';  $n = 17$ ) and HS34°C (Figure 3D';  $n = 32$ ) in comparison to 21°C (Figure 3A';  $n = 14$ ), indicating that MT density decreases. However, high temperatures can have an influence on the emission intensity of fluorescent proteins (Toca-Herrera et al., 2006). Hence, we cannot exclude that this reduction in emission intensity partially accounts for the decrease in pixel intensity seen here. Notably, the reduction in pixel intensity largely reverted at LT30°C (Figure 3C';  $n = 31$ ), implying that the biophysical emission reduction caused by heat does not have such a great impact in our setup, at least at 30°C. Moreover, the restoration of pixel intensities suggests the existence of an adaptation mechanism for MT bundling in response to heat. Further confirming an effect of heat on MTs, we specifically observed irregular spindle structures at 34°C but not at lower temperatures (Figure 3E), consistent with previous analyses (De Storme and Geelen, 2020; Lei et al., 2020).

Taken together, the quantitative but not qualitative changes of the typical meiotic MT configurations allow the

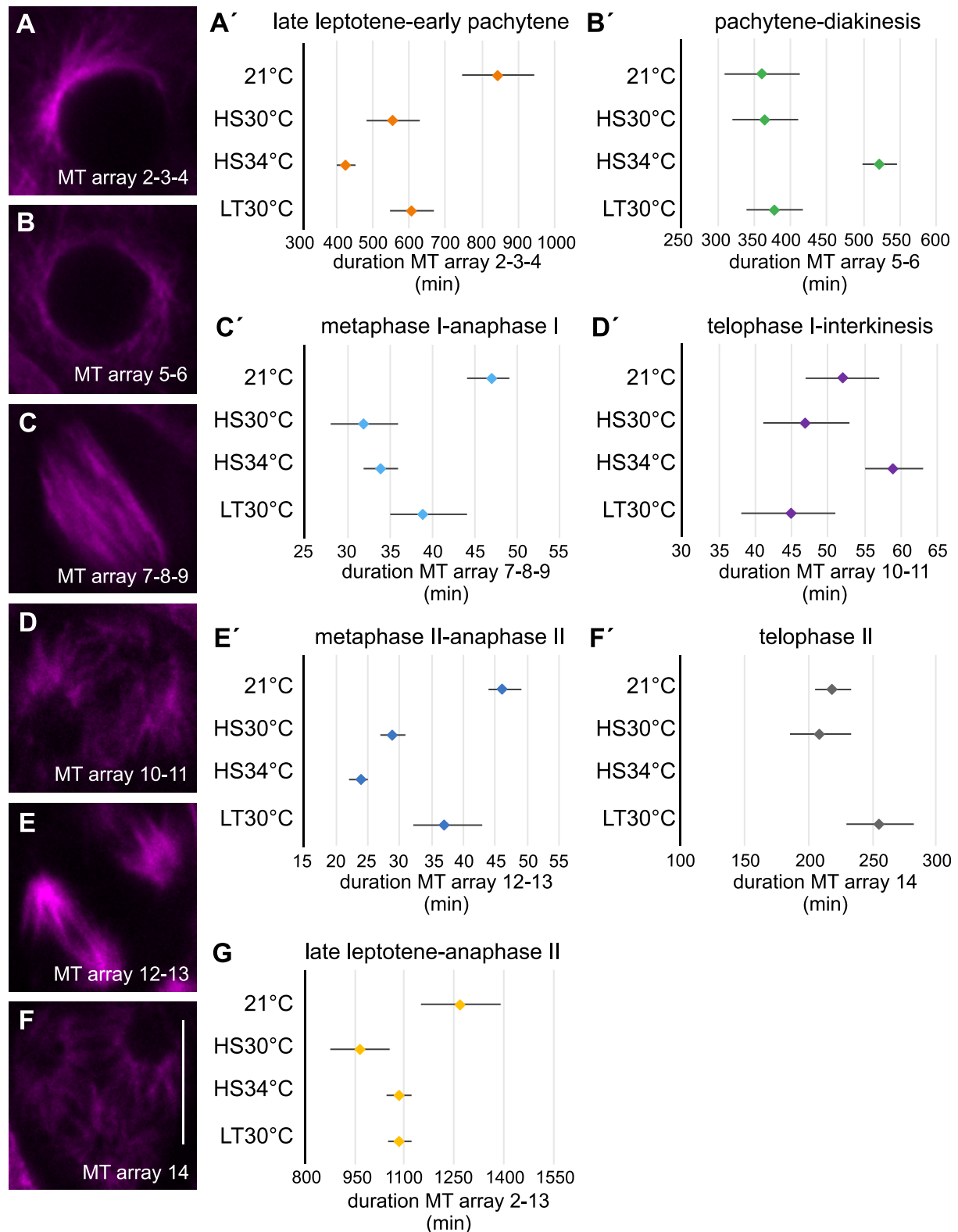
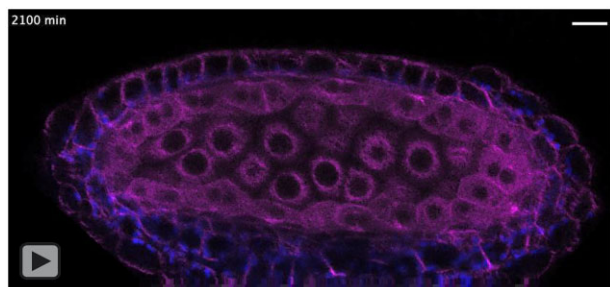
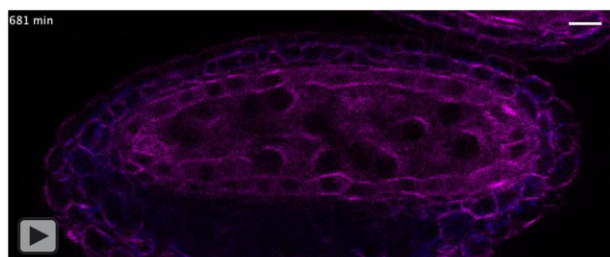


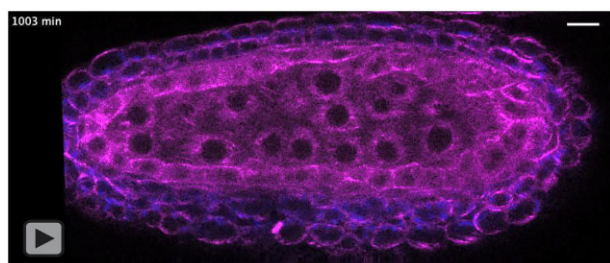
**Figure 2** Duration of meiotic phases based on MT array states. Confocal images of MT array states (A–F) and the corresponding predicted median times (in minutes) with 95% CIs in control (21°C) and heat conditions (HS30°C, HS34°C, and LT30°C) (A'–F'); (A, A'; orange) MT array state 2-3-4, late leptotene-early pachytene; (B, B'; green) MT array state 5-6, pachytene-diakinesis; (C, C'; light blue) MT array state 7-8-9, metaphase I-anaphase I; (D, D'; purple) MT array state 10-11, telophase I-interkinesis; (E, E'; dark blue) MT array state 12-13, metaphase II-anaphase II; (F, F'; gray) MT array state 14, telophase II. Scale bar, 10  $\mu$ m. G, Predicted median time (in minutes) of MT array states 2–13 with the 95% CI in control (21°C) and heat conditions (HS30°C, HS34°C, and LT30°C) (yellow).



**Movie 1.** Meiotic division of WT meiocytes at 21°C. Progression through meiosis of meiocytes in one WT pollen sac at 21°C. TagRFP-TUA5 in magenta, auto-fluorescence (chloroplasts) in blue. The meiocytes, localized in the central areas of the pollen sac, reside in a pre-meiotic stage at the beginning of the movie and undergo a complete meiotic program with the first and the second meiotic divisions until the formation of tetrads. Time is expressed in minutes; the interval between image acquisition is 10 min, time 0 corresponds to the start of image acquisition, and not to the start of meiosis. Scale bar, 10  $\mu$ m.

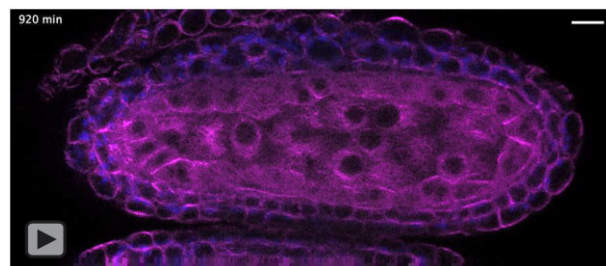


**Movie 2.** Meiotic division of WT meiocytes at HS30°C. Progression through meiosis of meiocytes in one WT pollen sac at HS30°C. TagRFP-TUA5 in magenta, auto-fluorescence (chloroplasts) in blue. Time is expressed in minutes; the interval between image acquisition is 10 min, time 0 corresponds to the start of heat shock treatment. Scale bar, 10  $\mu$ m.



**Movie 3.** Meiotic division of WT meiocytes at HS34°C. Progression through meiosis of meiocytes in one WT pollen sac at HS34°C. TagRFP-TUA5 in magenta, auto-fluorescence (chloroplasts) in blue. Time is expressed in minutes; the interval between image acquisition is 10 min, time 0 corresponds to the start of heat shock treatment. Scale bar, 10  $\mu$ m.

adoption of characteristic MT arrays for staging of meiosis during live cell imaging. At the same time, the quantitative effects on the MT arrays corroborate the previous finding that meiocytes successfully receive the heat treatment in our experimental set up.



**Movie 4.** Meiotic division of WT meiocytes at LT30°C. Progression through meiosis of meiocytes in one WT pollen sac at LT30°C. TagRFP-TUA5 in magenta, auto-fluorescence (chloroplasts) in blue. Time is expressed in minutes; the interval between image acquisition is 10 min, time 0 corresponds to the start of image acquisition. Scale bar, 10  $\mu$ m.

### Duration of meiosis under heat stress

The next challenge to overcome for the evaluation of meiotic progression at elevated temperatures was how to statistically compare the MT-based dissection of the different heat stress experiments with the control growth conditions. This was not a trivial question, since the analyses of meiocytes within one anther-sac cannot be regarded as statistically independent measurements but represent clustered data. In addition, the above-mentioned nature of defined meiotic stages gives rise to a multi-state nature of our dataset. Moreover, our measurements occasionally did not capture the exact start and/or end point (left, right, and/or interval-censored data) of an MT array state, since the observed anthers sometimes move out of the focal plane (but also occasionally move into focus again).

Including the combination of the three characteristics of our data, that is, clustered data, left/right, and/or interval censoring, as well as having a multistate nature, was not possible in one statistical model. Therefore, we reduced the multistate complexity of the analysis and built a separate model for each meiotic state, as defined by the MT configuration (see above) which also allowed us to simplify the mixture of left/right and/or interval-censored data with respect to the duration of each state to interval and right censoring. For detailed description of the models, please see the subsection “Statistical methods” in the section “Materials and methods”. With the imaging and evaluation system in hand, we then addressed the effect of HS30°C, HS34°C, and LT30°C treatments on the total length of meiosis.

The determination of the meiotic duration relied on defined start and end points of MT states (events). Since this is not possible for MT array state 1 (no start point), the first stage that could be temporally evaluated was thus MT array state 2–3–4. From a total of 59 movies, we first selected movies that covered all MT array states (2–14) under the four temperature regimes. Unfortunately for HS34°C, we were unable to reliably determine the end point of MT array state 14, as the fluorescent signal of the MTs became very poor, possibly due the fact that MTs are more diffusely organized at high temperature versus control conditions (described above, Figure 3), photo-bleaching after long time lapses as



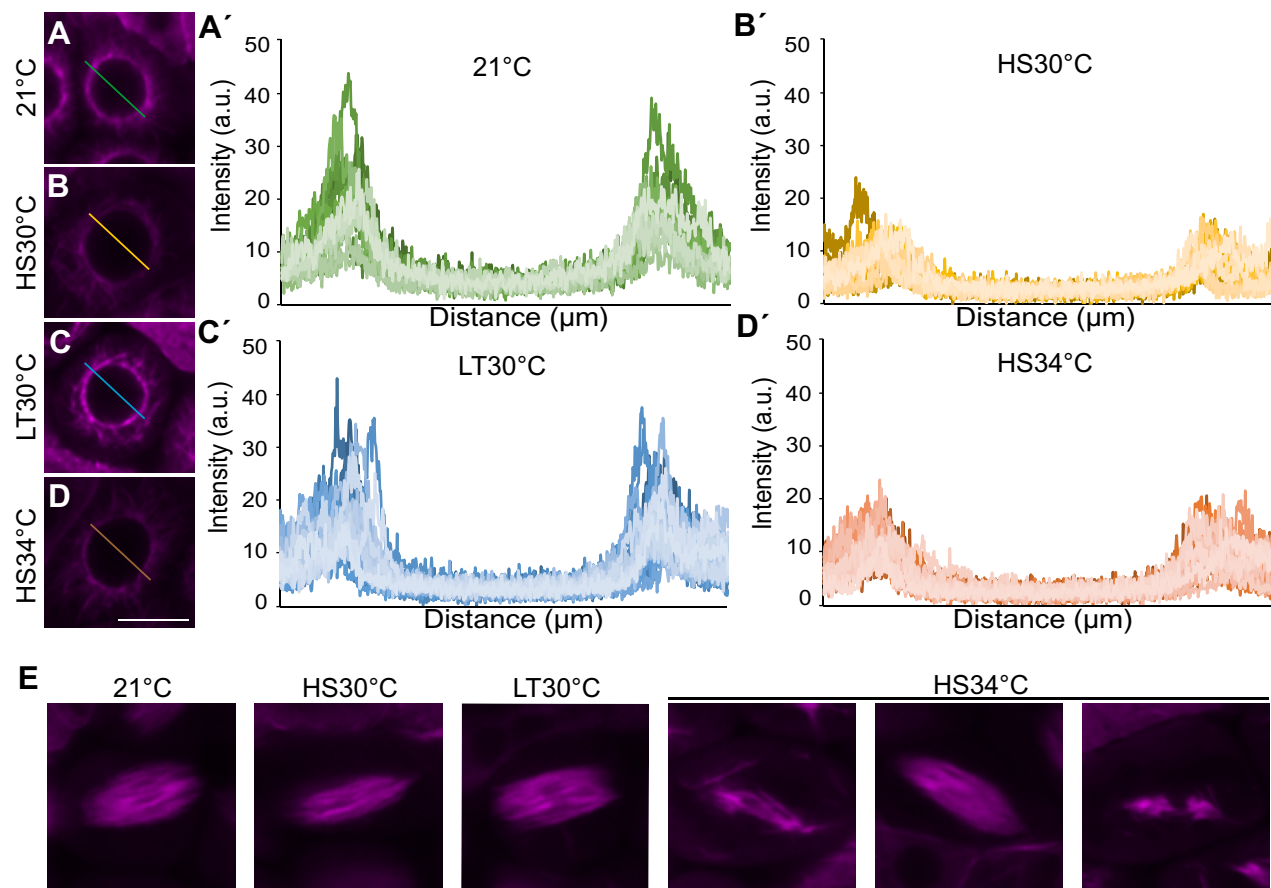


**Figure 3** MT array in the WT in control and heat stress conditions. A–D, Confocal images of meiocytes expressing *TagRFP-TUA5* (magenta) at MT array state 6 in control conditions of 21°C (A), heat shock conditions of HS30°C (B), LT30°C (C), and HS34°C (D). A'–D', Pixel intensity plot of a section crossing through the middle of the cell (distance in  $\mu\text{m}$ ) in MT array state 6 in 21°C (A', green,  $n = 14$ ), HS30°C (B', yellow,  $n = 17$ ), LT30°C (C', blue,  $n = 31$ ) and HS34°C (D', brown,  $n = 32$ ), section lines also highlighted in (A–D). E, Confocal images of meiocytes expressing *TagRFP-TUA5* (magenta) at MT array state 8–9 at 21°C, HS30°C, LT30°C, and HS34°C. Scale bar, 10  $\mu\text{m}$ .

well as possible effects on fluorescence emission at high temperatures.

To compare the overall meiotic duration at all heat conditions, we excluded MT array state 14 for this analysis and only considered movies capturing MT array states 2–13 (23 movies). We then built a separate parametric survival model for the complete duration (as described in “Materials and methods”), resulting in the total predicted median time, together with the 95% confidence interval (CI).

We determined that the duration of MT array states 2–13 at 21°C has a predicted median time of 1,271 min (or 21.2 h, 95% CI 1,151–1,390 min; Figure 2G; Supplemental Table S1). This value matched very well with previous analyses of the duration of male meiosis in Arabidopsis by pulse-chase experiments and live cell imaging, underscoring the robustness of our analysis and the reproducibility of meiotic progression at 21°C (Armstrong et al., 2003; Sanchez-Moran et al., 2007; Stronghill et al., 2014; Prusicki et al., 2019).

Next, we analyzed the duration of meiosis under the heat conditions, resulting in a predicted median time of 966 min (16.1 h, 95% CI 876–1,056 min) upon HS30°C; 1,086 min (18.1 h, 95% CI 1,048–1,124 min) upon HS34°C; and 1,086 min (18.1 h, 95% CI 1,050–1,122 min) upon

LT30°C (Figure 2G; Supplemental Table S1). Since the confidence intervals did not overlap, these data confirm previous observations that meiosis progresses faster under elevated temperatures in comparison to control conditions, also demonstrating that our experimental system can be faithfully used to study the effect of heat on meiosis (Wilson, 1959; Bennett et al., 1972; Stefani and Colonna, 1996; Draeger and Moore, 2017).

### Duration of individual meiotic phases under heat stress

The live cell imaging approach, together with the model-based calculation of the duration of the MT array states, allowed us then to target the main aim of this study, which was to obtain a detailed and phase-specific assessment of meiotic progression under elevated temperatures.

At 21°C, we observed a total of 206 meiocytes from 23 anther sacs and calculated the predicted median time per MT array state from those cells for which we could observe at least one time point in that specific state (Movie 1; Table 1; Supplemental Table S1). All reported median times were predictions from the respective parametric survival models (see “Materials and methods”). The predicted

**Table 1** Overview of the duration of the meiotic phases based on the MT array states

MT Array State		2-3-4		5-6		7-8-9		10-11		12-13		14	
Meiotic stage	Predicted time (in min)	Late leptotene-early pachytene	Pachytene-diakinesis	Metaphase I-anaphase I	Telophase I-interkinesis	Metaphase II-anaphase II	Telophase II	Median	95% CI	Median	95% CI	Median	95% CI
Treatment (n)													
21°C (206/23)	845	746	944	360	412	47	44	52	47	46	44	219	205
HS30°C (133/22)	556	485	628	365	411	32	28	47	41	29	27	209	185
HS34°C (188/26)	428	403	453	522	498	34	32	59	55	24	22	NA	NA
LT30°C (211/25)	609	550	667	378	416	39	35	45	38	37	32	256	230
<i>spo11</i> 21°C (224/27)	1,119	1,031	1,206	374	399	72	67	63	58	48	45	356	326
<i>dmc1</i> 21°C (157/24)	1,056	929	1,184	343	355	67	63	63	59	47	45	281	262
<i>msh4</i> 21°C (193/26)	951	861	1,040	314	299	67	63	59	56	49	46	274	253
<i>spo11</i> HS34°C (198/25)	626	572	681	412	393	35	32	54	49	23	21	NA	NA
<i>dmc1</i> HS34°C (160/19)	565	526	605	383	362	30	28	57	54	22	21	NA	NA
<i>msh4</i> HS34°C (116/17)	571	536	606	398	346	32	30	49	43	24	22	NA	NA
<i>atm</i> 21°C (228/28)	834	761	908	295	270	45	42	60	55	43	40	245	230
<i>atm</i> HS34°C (172/23)	702	640	764	350	330	31	29	55	50	26	23	NA	NA

Predicted median times and 95% CIs (in minutes) of MT array state 2-3-4 (late leptotene-early pachytene), MT array state 5-6 (pachytene-diakinesis), MT array state 7-8-9 (metaphase I-anaphase I), MT array state 10-11 (telophase I-interkinesis), MT array state 12-13 (metaphase II-anaphase II) and MT array state 14 (telophase II) of the WT at 21°C, HS30°C, HS34°C, LT30°C; recombination mutants *spo11*, *dmc1*, and *msh4* at 21°C and HS34°C and *atm* mutant at 21°C and HS34°C (n, number of cells/anther sacs observed). NA, not analyzed.

median time in MT array state 2-3-4 was 845 min (95% CI 746–944 min; [Figure 2A'](#)), followed by MT array state 5-6, with a predicted median time of 360 min (95% CI 309–412 min; [Figure 2B'](#)). MT array state 7-8-9 took place over 47 min (95% CI 44–49 min; [Figure 2C'](#)) while MT array state 10-11 spanned 52 min (95% CI 47–57 min; [Figure 2D'](#)). The second meiotic division then followed with a predicted median time of 46 min for MT array state 12-13 (95% CI 44–49 min; [Figure 2E'](#)), finishing the meiotic division with 219 min for MT array state 14 (95% CI 205–234 min; [Figure 2F'](#)).

Next, we analyzed male meiosis subjected to the three different temperature regimes in the same way. Accordingly, we observed a total of 133, 188, and 211 meiocytes from 22, 26, and 25 anther sacs were observed for HS30°C, HS34°C, and LT30°C, respectively. Again, we calculated the predicted median time per state from those cells for which we could observe at least one time point in that specific state ([Movies 2–4](#); [Table 1](#); [Supplemental Table S1](#)). The duration of MT array state 2-3-4 upon higher temperature was shorter compared to 21°C (845 min), with a predicted median time of 556 min upon HS30°C (95% CI 485–628 min), 428 min upon HS34°C (95% CI 403–453 min) and 609 min upon LT30°C (95% CI 550–667 min; [Figure 2A'](#)). The predicted median time in MT array state 2-3-4 at 21°C was therefore 289 min (95% CI 167–410 min) longer compared to HS30°C, 417 min (95% CI 315–519 min) longer compared to HS34°C and 236 min (95% CI 122–351 min) longer compared to LT30°C ([Supplemental Table S2](#)). These results demonstrated that the rise in temperature generally decreases the duration of this phase.

In the next phase, MT array state 5-6 exhibited a strikingly different behavior. While upon exposure to HS30°C and LT30°C, the predicted median time was 365 min (95% CI 319–411 min) and 378 min (95% CI 340–416 min), respectively, HS34°C resulted in a predicted median of 522 min (95% CI 498–546 min; [Figure 2B'](#)). The duration of this phase at HS34°C was thus longer compared to 21°C (360 min), with a difference of 162 min (95% CI 104–219 min; [Supplemental Table S2](#)), presenting a prolongation of ~2.7 h.

After NEB, the meiocytes undergo the first round of chromosome segregation, that is, MT array state 7-8-9, with a predicted median time of 32 min (95% CI 28–36 min) upon HS30°C, 34 min (95% CI 32–36 min) upon HS34°C and 39 min (95% CI 35–44 min) upon LT30°C, which is shorter compared to 21°C (47 min; [Figure 2C'](#), for details on differences see [Supplemental Table S2](#)).

The following MT array state 10-11 spanned 47 min (95% CI 41–53 min) upon HS30°C, 59 min (95% CI 55–63 min) upon HS34°C and 45 min (95% CI 38–51 min) upon LT30°C ([Figure 2D'](#)), with only the duration at HS34°C being longer by 7 min (95% CI 0.6–13 min) than at 21°C ([Supplemental Table S2](#)).

Upon HS30°C, HS34°C, and LT30°C, the second round of chromosome segregation, MT array state 12-13, spanned 29 min (95% CI 27–31 min), 24 min (95% CI 22–25 min), and

37 min (95% CI 32–43 min), respectively (Figure 2E'). These durations were shorter compared to 21°C (46 min, for details on differences see Supplemental Table S2).

We estimated the end of the meiotic division upon heat treatment by using MT array state 14, which spanned 209 min (95% CI 185–233 min) upon HS30°C and 256 min (95% CI 230–282 min) upon LT30°C (Figure 2F'). Notably, the pairwise comparison of 21°C and LT30°C showed an increase of 9 min (95% CI 3–15 min; Supplemental Table S2).

Currently, the underlying reasons for the above-identified alterations in meiotic durations under different temperatures are not clear and await further investigations. In the following, we focused on one of the most striking and unexpected observations: the temporal increase of late prophase at HS34°C.

### Exposure to high temperature causes chromosomal defects during meiosis

To investigate the prolongation of late prophase at 34°C (Figure 2B') in more detail, we first performed chromosome spreads from fixed flower buds exposed to the different temperature regimes. At control growth conditions, decondensed chromatin becomes organized into chromosomes that will gradually condense during early prophase I and reach a fully paired state at pachytene. The paired homologs condense further, where chiasmata hold homologs together, finally reaching the highest condensed state at diakinesis with the formation of five bivalents that align at the metaphase plate during metaphase I (Supplemental Figure S2A). At both HS30°C ( $n = 136$ ) and LT30°C ( $n = 130$ ), homologs condensed and fully paired. Occasionally, two or more bivalents appeared to be entangled at diakinesis ( $n = 36/73$  and  $n = 52/81$ , respectively) and metaphase I, forming chromosome bridges ( $n = 26/65$  and  $n = 11/25$ , respectively), suggesting interconnected nonhomologous chromosomes. In addition, we infrequently observed chromosome fragments ( $n = 3/81$  at LT30°C) and univalents (at diakinesis:  $n = 2/73$  and  $n = 1/81$ , at metaphase  $n = 4/65$  and  $n = 2/25$ , respectively; Supplemental Figure S2, B and C). In contrast to 21°C and 30°C, we failed to detect fully paired homologs at 34°C ( $n = 115$ ). Furthermore, chromosome spreads of cells in diakinesis and metaphase I at 34°C revealed the formation of mainly 10 univalents ( $n = 64$  and  $n = 17$ , respectively). In addition, chromosome bridges were visible between both homologs and nonhomologous chromosomes ( $n = 33/64$  and  $n = 11/17$ , respectively; Supplemental Figure S2D).

Thus, consistent with previous analyses in fission yeast (*Saccharomyces pombe*), barley, and Arabidopsis, high temperature caused recombination defects that increase with rising temperatures (Higgins et al., 2012; Bomblies et al., 2015; Phillips et al., 2015; Morgan et al., 2017; Modliszewski et al., 2018; Brown et al., 2020; De Storme and Geelen, 2020).

### Synaptonemal complex formation is defective at 34°C

Given the central role of the formation of the chromosome axis for pairing and meiotic recombination, we next analyzed the localization of the previously generated reporters ASYNAPTIC 1 fused to RFP (ASY1-RFP) and ZIPPER 1b fused to the green fluorescent protein (ZYP1b-GFP) upon 30°C and 34°C (Yang et al., 2019, 2020). ASY1 is a chromosome axis-associated protein that plays a major role in the initiation of synapsis and recombination (Caryl et al., 2000; Armstrong et al., 2002; Sanchez-Moran et al., 2007). ZYP1b is a component of the transversal filament of the synaptonemal complex (SC) (Higgins et al., 2005; Osman et al., 2006; Capilla-Perez et al., 2021; France et al., 2021).

Under the standard growth conditions of 21°C, ASY1 localized to the chromosome axis from early leptotene to pachytene. During zygotene, when the formation of the SC is initiated, ASY1 became largely depleted from the chromosome axis, while the ZYP1b signal started to appear on chromosomes and gradually expanded to form a linear structure ( $n = 99$ ), resulting in the labeling of the entire chromosome axis at pachytene ( $n = 39$ ; Figure 4A).

At the high temperatures of 30°C and 34°C, the localization of ASY1 at the chromosome axis was unaffected and ZYP1b started to form short linear stretches at the chromosome axis during zygotene ( $n = 84$  and  $n = 93$ , respectively) (Figure 4, B and C). At 30°C, ZYP1b continued to label the full length of the axis ( $n = 40$ ), in contrast to 34°C, at which temperature we only detected small stretches of ZYP1b signal ( $n = 68$ ), suggesting that ZYP1b loading is initiated properly but discontinues (Figure 4, B and C). This result was in accordance with previous findings in nematodes, barley, and wild garlic showing that synapsis is obstructed upon high temperature exposure, leading to the formation of abnormal structures called polycomplexes (Loidl, 1989; Higgins et al., 2012; Bilgir et al., 2013).

### Defects in early prophase I cause an elongation of pachytene/diakinesis

Seeing defective SC formation at 34°C, we asked whether events between zygotene and pachytene were particularly sensitive to heat stress and hence, responsible for the delay of NEB. Therefore, we specifically applied heat stress only from MT state 2-3-4 (zygotene) onward (called late HS) and compared the effect of this treatment to the previously applied heat shock before MT state 1, that is, from premeiosis-leptotene onward (referred to as early HS), by live cell imaging. Since we showed above that male meiocytes perceive heat stress in < 15 min, we were confident that a late heat shock would allow us to distinguish the temperature effects on early versus late prophase faithfully.

We calculated the predicted median time of MT array state 5-6 as described above and performed a comparison between early and late HS. We did not observe a difference between HS30°C applied early or late (difference of 52 min [95% CI –11 to 115 min]), with a predicted median time of 313 min for MT array state 5-6 at late HS30°C (95% CI 270–355 min;



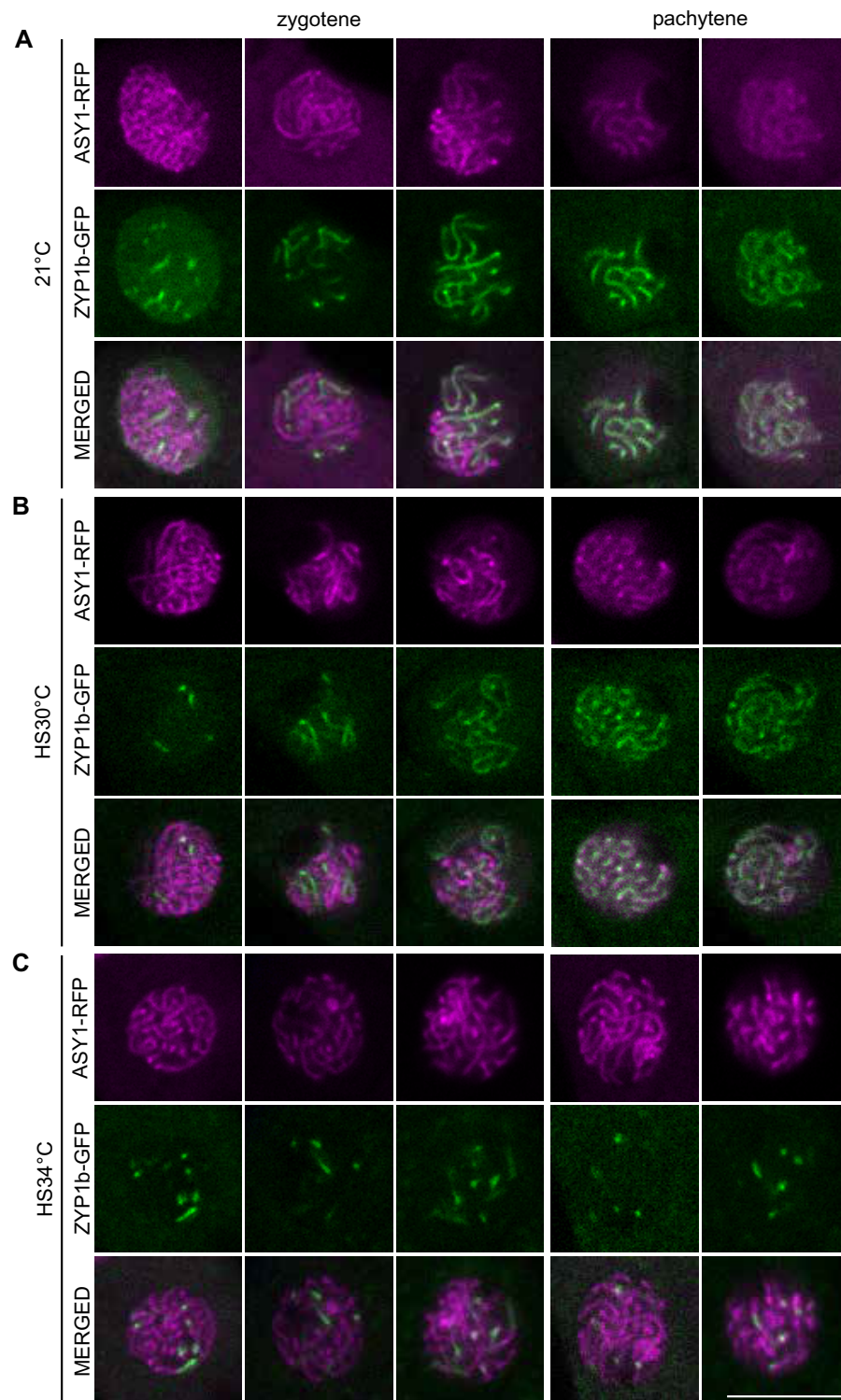


**Figure 4** Localization of the synaptonemal complex elements ASY1 and ZYP1b upon heat stress. Confocal images of the nucleus of meiocytes at 21°C (A), HS30°C (B), and HS34°C (C) of SC elements ASY1-RFP (magenta, first row) and ZYP1b-GFP (green, second row) separately and merged (third row) at zygotene (Columns 1–3) and pachytene (Columns 4 and 5). Scale bar, 10  $\mu$ m.

Figure 5; Supplemental Tables S1 and S2). Remarkably, the MT array state 5-6 was not extended when we applied HS34°C late in prophase I, since we obtained a predicted median time of 393 min (95% CI 349–437 min; Figure 5; Supplemental Table S1, for details on differences see Supplemental Table S2).

This observation suggested that the prolongation of MT array state 5-6 is predominantly due to temperature-sensitive events in early steps in prophase I, for example, the initiation of meiotic recombination, that subsequently affect the duration of pachytene/diakinesis.

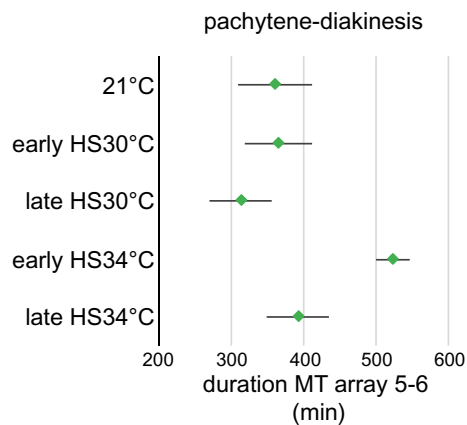


**Figure 5** Effect of early and late heat shock on the duration of MT array state 5-6. Predicted median time (in minutes) with 95% CIs of pachytene-diakinesis (MT array state 5-6; green) at 21°C, early HS30°C versus late HS30°C and early HS34°C versus late HS34°C. 21°C, early HS30°C, and early HS34°C, as shown in [Figure 2B'](#).

### Loss of recombination per se does not cause the elongation of pachytene/diakinesis

To address to what degree a failure of recombination causes a pachytene/diakinesis delay, as observed in animals ([Crichton et al., 2018](#)), we first made use of the well-characterized *spo11-1* mutant, in which recombination is completely abolished due to a failure to form DSBs ([Grelon et al., 2001](#); [Hartung et al., 2007](#)). We introduced the *TagRFP-TUA5* reporter in *spo11-1*, allowing us to follow meiotic progression by using live cell imaging and MT state-based determination of meiotic phases from 27 anther sacs with a total of 224 observed meiocytes ([Supplemental Movie S1](#); [Table 1](#); [Supplemental Table S1](#)).

Interestingly and not previously recognized, early prophase (MT array state 2-3-4, late leptotene to early pachytene) was clearly extended in *spo11-1* mutants, with a predicted median time of 1,119 min (95% CI 1,031–1,206 min; [Figure 6A](#)), that is, a difference of 274 min (95% CI 143–405 min) with the wild-type (WT; [Supplemental Table S2](#)).

Important for this study, the duration of MT array state 5-6 in *spo11-1* (predicted median time of 374 min [95% CI 349–399 min], [Figure 6B](#)) was not relevantly different compared to the WT (with a difference of 14 min [95% CI –36 to 64 min]; [Supplemental Table S2](#)). This result suggested that the complete loss of recombination caused by the absence of DSBs in the *spo11-1* mutant does not lead to a prolongation of MT array state 5-6 at 21°C.

After prophase I, the meiotic division in *spo11-1* mutants continued with a predicted median time of 72 min (95% CI 67–76 min) for MT array state 7-8-9, followed by MT array state 10-11 with 63 min (95% CI 58–67 min), MT array state 12-13 with 48 min (95% CI 45–52 min), and finally MT array state 14 with 356 min (95% CI 326–385 min) ([Supplemental Figure S4](#)). Of note, the durations of MT array state 7-8-9, MT array state 10-11, and MT array state 14 in the *spo11-1* mutant were slightly longer compared to the WT (for details on differences, see [Supplemental Table S2](#)).

Next, we asked whether a prolongation of MT array state 5-6 depend on homologous recombination (HR) repair by following meiosis in *dmc1* mutants in which we introduced the *TagRFP-TUA5* reporter and observed a total of 157 meiocytes from 24 anther sacs ([Supplemental Movie S2](#); [Table 1](#); [Supplemental Table S1](#)). In *dmc1* mutants, DSBs are repaired through the sister chromatid of the same chromosome in an HR-dependent manner ([Kurzbaue et al., 2012](#)). We calculated the predicted median time per state, which returned a duration of 1,056 min for MT array state 2-3-4 (95% CI 929–1,184 min; [Figure 6A](#)), which was longer relative to the WT (with a difference of 211 min [95% CI 36–386 min]; [Supplemental Table S2](#)) and resembling the extension of this phase seen in *spo11-1*. Thus, loss of early recombination steps appeared to trigger a prolongation of early meiosis in Arabidopsis, although it is currently not clear whether the extensions in *spo11-1* and *dmc1* have the same underlying reason. For MT array state 5-6 in *dmc1*, we determined a similar duration of 343 min (95% CI 331–355 min; [Figure 6B](#)) compared to the WT (360 min; [Figure 2B'](#)); hence, we also did not observe a temporal extension of MT array state 5-6 for *dmc1* mutants (for details on differences see [Supplemental Table S2](#)). The meiotic division continued with a predicted median time of 67 min (95% CI 63–71 min) for MT array state 7-8-9. MT array state 10-11 took 63 min (95% CI 59–67 min), MT array state 12-13 lasted 47 min (95% CI 45–49 min), and MT array state 14 spanned 281 min (95% CI 262–301 min; [Supplemental Figure S4](#)). All these subsequent phases had durations similar to those in *spo11-1* (for details on differences, see [Supplemental Table S2](#)).

Finally, we tested whether a failure to resolve recombination intermediates as Type I COs might be responsible for the delayed onset of NEB, using *msh4* mutants harboring the *TagRFP-TUA5* reporter ([Supplemental Movie S3](#)). Accordingly, we observed a total of 193 meiocytes from 26 anther sacs and calculated the predicted median time for every stage ([Table 1](#); [Supplemental Table S1](#)). In *msh4*, MT array state 2-3-4 took 951 min (95% CI 861–1,040 min; [Figure 6A](#)). This duration was not relevantly different from that of the WT (with a difference of 106 min [95% CI –18 to 230 min]; [Supplemental Table S2](#)) but lied in between the CI for the WT and the CI for *spo11-1* and *dmc1* mutants. Hence, it was difficult at this point to judge from this dataset whether this extension was biologically relevant in comparison to the WT and resembled the situation found in the other two recombination mutants.

Subsequently, we determined a duration of 314 min (95% CI 299–329 min) in *msh4* for MT array state 5-6 ([Figure 6B](#)). The meiotic division continued with an extended MT array state 7-8-9 for 67 min (95% CI 65–72 min; [Supplemental Figure S3A](#)) compared to the WT (with a difference of 21 min [95% CI 16–25 min]; [Supplemental Table S2](#)), which was similar to the extension seen in *spo11-1* and *dmc1*. Next, MT array state 10-11 in *msh4* lasted 59 min (95% CI

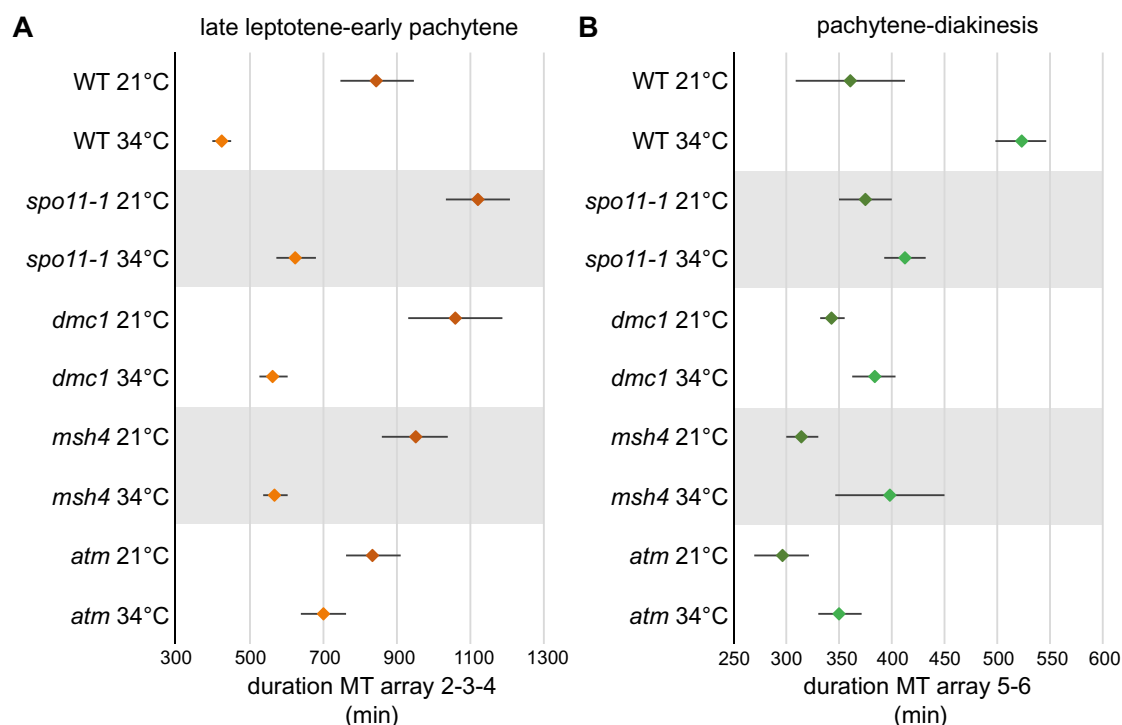


**Figure 6** Duration of prophase in the recombination mutants *spo11-1*, *dmc1*, *msh4*, and *atm* at 21°C and HS34°C. A and B, Predicted median times (in minutes) with 95% CI of (A) late leptotene-early pachytene (MT array state 2-3-4; orange) and (B) pachytene-diakinesis (MT array state 5-6; green) in the WT (as shown in Figure 2, A' and B') and recombination mutants *spo11-1*, *dmc1*, *msh4*, and *atm* at 21°C and HS34°C.

56–63 min), MT array state 12-13 took 49 min (95% CI 46–52 min) and finally, MT array state 14 spanned 274 min (95% CI 253–294 min; Supplemental Figure S3, B–D). Thus, all recombination mutants tested displayed a similar duration of MT array states 5-6 and 12-13, compared to the WT (for details on differences, see Supplemental Table S2).

Yet, *msh4* mutants progressed through pachytene/diakinesis as WT plants at 21°C. Previous 5'-bromo-2'-deoxyuridine (BrdU) labeling experiments in *Arabidopsis* had shown a delay of 8 h for S-phase to the end of prophase I in *msh4* mutants that we did not see in our experiments. Notably, our time predictions did not include meiotic S-phase and early leptotene, where MSH4 is known to start appearing as numerous foci on the axes (Higgins et al., 2004). Thus, considering all data, it is likely that *Arabidopsis msh4* mutants are particularly delayed in the premeiotic S-phase given its known role in repairing DNA base-pair mismatches, which take place during DNA replication (Santucci-Darmanin et al., 2002).

Taken together, these results indicated that the loss of recombination per se does not cause the elongation of the MT array state 5-6 seen in WT meiocytes at 34°C.

### Prolongation of MT array state 5-6 is largely recombination-dependent

To then investigate the role of the recombination pathway on the elongation of MT array state 5-6 upon very high temperature heat stress, we characterized a total of 198 meiocytes from 25 anther sacs and analyzed the duration of

this phase in *spo11-1* mutants at HS34°C (Supplemental Movie S4; Table 1; Supplemental Table S1). As for heat shock treatments of WT meiocytes, we used only flower buds in MT array state 1 to model the duration of the different meiotic states at HS34°C.

The MT array state 2-3-4 of *spo11-1* had a predicted median time of 626 min (95% CI 572–681 min; Figure 6A), which was shorter in duration compared to *spo11-1* at 21°C (with a difference of 492 min [95% CI 389–595 min; Supplemental Table S2]), showing a similar reduction of 417 min (95% CI 315–519 min; Supplemental Table S2) as described for WT meiocytes. Notably, the elongation of MT array state 5-6 seen in the WT at HS34°C (a difference of 162 min [95% CI 104–219 min] compared to 21°C; Figure 2B'; Supplemental Table S2) was not found in *spo11-1* mutant at HS34°C, with a predicted median time of 412 min (95% CI 393–431 min; Figure 6B), compared to *spo11-1* at 21°C (a difference of 38 min [95% CI 6–70 min; Supplemental Table S2]). Further, MT array state 7-8-9 took 35 min (95% CI 32–38 min), MT array state 10-11 spanned 54 min (95% CI 49–58 min) and MT array state 12-13 lasted 23 min (95% CI 21–26 min; Supplemental Figure S3, A–C). All these states, with the exception of MT array states 2-3-4 and 5-6, were not relevantly different compared to the WT at HS34°C (Supplemental Table S2). Furthermore, all these states showed a reduction similar in length to that described for the WT at HS34°C versus 21°C. For MT array state 14 in *spo11-1* at HS34°C, we did not calculate median time, as we did not for the WT at HS34°C.



This result suggested that the delay in the WT at the very high temperature of 34°C is not due to the absence of recombination, but rather due to aberrant recombination intermediates; in their absence, as in *spo11-1* mutants, meiosis progresses without delay. To further explore this possibility, we next observed a total of 160 *dmc1* and 116 *msh4* meiocytes from 19 and 17 anther sacs, respectively, and measured the duration of MT array state 5-6 at HS34°C (Supplemental Movies S5 and S6; Table 1; Supplemental Table S1). The predicted median time of MT array state 2-3-4 upon HS34°C was 565 min (95% CI 526–605 min) for *dmc1* mutants and 571 min (95% CI 536–606 min) for *msh4* mutants, representing a decrease relative to their median time at 21°C (Figure 6A, for details on differences, see Supplemental Table S2). The predicted median time of MT array state 5-6 of *dmc1* and *msh4* at HS34°C was 383 min (95% CI 362–403 min) and 398 min (95% CI 346–450 min), respectively (Figure 6B).

Finally, *dmc1* and *msh4* mutant plants continued meiosis at HS34°C, with MT array state 7-8-9 of 30 min (95% CI 28–32 min) and 32 min (95% CI 30–34 min); MT array state 10-11 lasting 57 min (95% CI 54–60 min) and 49 min (95% CI 43–55 min); and MT array state 12-13 taking 22 min (95% CI 21–23 min) and 24 min (95% CI 22–26 min), respectively (Supplemental Figure S3, A–C). Similar to the WT and *spo11-1* at HS34°C, we were unable to obtain a predicted median time for the MT array state 14.

In summary, the analyses of *dmc1* and *msh4* together with the data obtained for *spo11-1* strongly suggested that aberrant recombination structures are largely responsible for the delay of pachytene/diakinesis observed in the WT. However, compared to the timing of these three mutants at 21°C, their durations at 34°C were also slightly longer (Figure 6B; Supplemental Table S2). Thus, it is also likely that an unknown and recombination-independent component appears to contribute to the observed elongation.

### A specialized pachytene checkpoint in Arabidopsis

Our results illustrating the prolongation of pachytene/diakinesis were reminiscent of the pachytene checkpoint of animals and yeast. However, the observation that mutants devoid of recombination nevertheless go through meiosis in plants (as quantified above) has previously raised the hypothesis that plants do not have a pachytene checkpoint (Couteau et al., 1999; Grelon et al., 2001; Caryl et al., 2003; Higgins et al., 2004; Li et al., 2004, 2009b; Jones and Franklin, 2008). A central executor of the pachytene checkpoint in yeast and animals is the checkpoint kinase ATM (Lange et al., 2011; Pacheco et al., 2015; Penedos et al., 2015). ATM is highly conserved and also plays a major role in meiosis in Arabidopsis, for instance for the repair of DSBs (Garcia et al., 2003; Li et al., 2004; Lange et al., 2011; Yao et al., 2020; Kurzbaue et al., 2021).

We hypothesized that if the observed extension of MT array state 5-6 in the WT is due to a pachytene checkpoint, *atm* mutants should also suppress this extension. To test this idea, we introduced the *TagRFP-TUA5* reporter in the

*atm* mutant and followed meiotic progression at 21°C and HS34°C using live cell imaging by observing a total of 228 and 172 meiocytes from 28 and 23 anther sacs, respectively. We then determined the duration of the MT array states as described before (Supplemental Movies S7 and S8; Table 1; Supplemental Table S1).

At 21°C, MT array state 2-3-4 lasted 834 min (95% CI 761–908 min) while MT array state 5-6 took 295 min (95% CI 270–321 min; Figure 6) in the *atm* mutant. Thus, *atm* meiocytes progressed even faster than the WT through MT array state 5-6 (with a difference of 65 min [95% CI 7–123 min]; Supplemental Table S2), hinting at a possible role in prolonging pachytene/diakinesis even under control conditions. Next, we measured the duration of MT array state 7-8-9 at 45 min (95% CI 42–49 min), MT array state 10-11 at 60 min (95% CI 55–66 min), MT array state 12-13 at 43 min (95% CI 40–46 min) and MT array state 14 at 245 min (95% CI 230–260 min; Supplemental Figure S3). Thus, MT array state 10-11 and 14 were slightly longer than in the WT (for details on differences, see Supplemental Table S2). The reason for this extension is not clear at the moment.

Upon exposure to HS34°C, MT array state 2-3-4 had a predicted median time of 702 min (95% CI 640–764 min); strikingly, the prolongation of MT array state 5-6 seen in the WT was largely abolished, as the difference between *atm* mutants HS34°C and 21°C was only 55 min (95% CI 22–87 min) versus a difference of 162 min (95% CI 104–219 min) between the WT at HS34°C and 21°C (Figure 6; Supplemental Table S2).

The durations of the other MT array states were not relevantly different compared to the WT at HS34°C, that is, MT array state 7-8-9 lasted 31 min (95% CI 29–33 min), MT array state 10-11 took 55 min (95% CI 50–60 min), and MT array state 12-13 spanned 26 min (95% CI 23–28 min) (Supplemental Figure S3, A–C, for details on differences, see Supplemental Table S2). The duration of MT array state 14 at HS34°C could not be determined as before.

These results implicated ATM in the prolongation of pachytene/diakinesis at HS34°C. Given the similarities in extension of pachytene/diakinesis, that is, dependency on recombination and the involvement of ATM, we conclude that Arabidopsis and likely other plants do have a specialized variant of the pachytene checkpoint that relies on the action of ATM and possibly other regulators to monitor aberrant recombination intermediates at high temperatures but, in contrast to animals, not the absence of recombination itself.

## Discussion

More than 50 years ago, the consequences of high temperature on plant development in general and on meiosis, in particular, were already being studied (Pao and Li, 1948; Dowrick, 1957; Wilson, 1959). Due to the dire outlook caused by climate change, research on the influence of temperature on meiosis has been revived. Previous and current studies have relied on the analysis of fixed samples and

obtained important insights into the duration of meiosis and meiotic recombination patterns at elevated temperatures (Modliszewski et al., 2018; Brown et al., 2020; De Storme and Geelen, 2020). Here, we followed a complementary approach by following meiosis by time-lapse live cell imaging. This method allowed us to obtain a highly temporally resolved dissection of meiotic progression in which we compared the effects of three heat stress treatments, that is, a heat shock at 30°C and 34°C and a long-term (1 week) treatment at 30°C in comparison to the control temperature of 21°C. Notably, this work provided novel insights into the effects of temperature on recombination as well as meiotic progression and set the stage for revising a current dogma in the field.

### Formation of SGs during meiosis

Heat stress induces a multitude of cellular responses, including the inhibition of general translation and the formation of SGs, which are proposed to function as transient places for both storage and degradation of proteins and mRNAs during stress resulting in translational re-programming. The formation of SGs is thought to be especially important for the re-initiation of translation upon recovery from the stress condition, as reviewed previously (Anderson and Kedersha, 2002, 2008; Buchan and Parker, 2009). In mice spermatocytes, SGs were previously shown to be formed after heat treatment (42°C) and these SGs contained for instance Deleted in azoospermia-like (DAZL), an RNA-binding protein that interacts with the SC, is involved in mRNA transport and is proposed to function as a translational activator (Kim et al., 2012).

By fluorescently labeling the major cell cycle regulator of Arabidopsis CDKA;1, we showed here that meiocytes in Arabidopsis also form SGs at 30°C and 34°C. CDKA;1 was previously demonstrated along with several other proteins, like MITOGEN-ACTIVATED PROTEIN KINASE 3 and the TARGET OF RAPAMYCIN COMPLEX 1, to be present in SGs of heat-stressed seedlings (Kosmacz et al., 2019). The presence of CDKA;1 in SGs was hypothesized to allow a cell to resume cell division activity in Arabidopsis after attenuation of the stress (Kosmacz et al., 2019). CDKs typically require a co-factor, called cyclin, for their activity; in budding yeast, the RNA-binding protein WHISKEY 8 (WHI8) was shown to bind to and recruit the mRNA of the cyclin CLN3 to SGs upon heat stress, causing the inhibition of CLN3 mRNA translation (Yahya et al., 2021). Interestingly, Cell Division Cycle 28, the homolog of CDKA;1 in budding yeast, is itself also recruited to SGs by WHI8 and has been found to play an important role in SG dissolution and the translation of SG-recruited mRNAs, such as for CLN3, upon release from stress.

Might Arabidopsis CDKA;1 also be a mediator of SG dissolution and subsequent re-initiation of translation? Interestingly, many proteins related to translation were previously identified as putative CDKA;1 substrates (Pusch et al., 2011). A pivotal role of translational control for the abundance of proteins in meiosis has been established in

several organisms including budding yeast (Brar et al., 2012), raising the possibility that translational regulation of meiosis in Arabidopsis is also present and likely controlled by CDK activity.

The appearance of CDKA;1 in SGs allowed us to faithfully confirm the application of the heat stress in meiocytes. On the one hand, we were able to show that the heat stress reaches meiocytes relatively fast, that is, in <15 min. Thus, all our imaging started when meiocytes are already exposed to the desired applied temperature in our set-up. On the other hand, we observed that SGs are not regularly found at 30°C. Thus, the appearance of SGs highlights meiocytes experiencing temperature stress >30°C. Since SGs formed rapidly at 34°C, we hypothesize that the heat stress at 30°C also reaches meiocytes in a similar time frame, offering us the confidence that we are looking at an immediate effect of the high temperature rather than a ramping effect over a long period. We anticipate that the formation of CDKA;1-containing SGs may be used as a general readout to study heat stress in other plant tissues and possibly other plant species as well.

Interestingly, the localization of CDKA;1 to SGs was stage-specific and its SG localization was only observed from pachytene onward but not earlier in meiosis. Notably, DAZL also shows a stage-specific localization to SGs in mice spermatocytes and is recruited to SGs only during pachytene in response to heat, coinciding with its highest accumulation level (Kim et al., 2012). In comparison, CDKA;1 dynamically localized to the nucleus and the cytoplasm and the formation of CDKA;1-positive SGs appeared when its cytoplasmic portion was the highest. Therefore, whether the formation of CDKA;1-positive SGs is dependent on its high cytoplasmic concentration or whether the presence of CDKA;1 in SGs relies on other meiotic stage-specific parameters needs to be determined. Conversely, it is also not clear whether non-CDKA;1-containing SGs form prior to pachytene.

### Heat and meiotic progression

The changes in duration for meiosis upon high temperatures were studied in several plant species including Arabidopsis, barley, wheat, *Dasypyrum villosum* (L.) P. candargy and bluebell (*Hyacinthoides non-scripta*; Wilson, 1959; Bennett et al., 1972; Stefani and Colonna, 1996; Higgins et al., 2012; Draeger and Moore, 2017). These studies have relied on static analyses of fixed material, for example, anther fixation and staging before and after a certain time interval or BrdU pulse labeling followed by the analysis of meiotic chromosome figures (Bennett et al., 1972; Armstrong et al., 2003). These studies concluded that the duration of meiosis hastens at high temperatures. Here, we confirmed this general trend of increased meiotic speed at high temperatures. However, our live cell imaging approach allowed us to follow meiotic progression with great depth, generating quantitative data that can be statistically analyzed, which led to the finding that not all meiotic phases respond equally to an increase in temperature. For instance, the progression into interkinesis in the WT was considerably delayed at 34°C. The underlying

reasons for this delay are currently unclear, but it is an interesting speculation that there are several as yet recognized control point/checkpoints during meiosis.

Most strikingly, we discovered that pachytene/diakinesis are in particular extended at 34°C when compared to control conditions at 21°C, as seen by a considerable prolongation of the time of NEB. This observation opens the door to study which regulators and/or processes are sensitive to heat, for instance with respect to controlling NEB. However, how NEB is controlled in plants is still an enigma, especially since lamins do not appear to be conserved in plants (Fiserova and Goldberg, 2010; Ciska and Moreno Diaz de la Espina, 2013). Notably, NEB likely represents a gate in meiotic progression. Chromosomes are strong MT organizing structures in plants (Lee and Liu, 2019), and once the nuclear envelope is broken down, the MT array that is enriched around the nucleus quickly connects to the chromosomes and organizes itself into a spindle (Prusicki et al., 2019). Thus, a delay of NEB represents a physical barrier that provides additional time to complete and/or correct processes in the reaction environment of the nucleus before chromosomes start to be moved in the cell.

### Heat and meiotic recombination

The observed extension of pachytene/diakinesis under heat stress prompted us to genetically and temporally dissect this effect. An obvious cause for the observed prolongation was altered meiotic recombination, supported by this study and previous analyses in Arabidopsis and barley of meiotic chromosome configurations (Higgins et al., 2012; De Storme and Geelen, 2020; Hedhly et al., 2020). Using mutants in genes that control different steps in the meiotic recombination process, like *spo11-1*, *dmc1*, and *msh4*, we showed that the extension of pachytene/diakinesis is recombination-dependent, that is, the extension of pachytene/diakinesis was lost in these mutants at 34°C. Notably, these mutants, when grown under nonstress conditions at 21°C, did not display a relevant prolongation of late pachytene (MT array state 5-6) in a detectable manner with our assays. This result stands in contrast to animals where loss of recombination, for example, in *dmc1* mutant mice, triggers meiotic arrest and subsequently induces cell death (Roeder and Bailis, 2000; de Rooij and de Boer, 2003; Barchi et al., 2005).

To further narrow down the origin of the elongation of pachytene/diakinesis, we applied heat stress only around zygotene, that is, up to 17 h later than in our first sets of experiments. Importantly, this late heat stress did not cause a prolongation, suggesting that recombination appears to be affected prior to SC formation. This observation is interesting, since earlier work in barley and *A. ursinum* indicated that the SC is severely affected by heat, leading to so-called polycomplexes in which transverse filaments become laterally connected; a study in *C. elegans* suggested that ZYP1 aggregation upon high temperature primarily reflects a failure of SC assembly (Loidl, 1989; Higgins et al., 2012; Bilgir et al., 2013). In addition, temporal dissection of heat stress on spermatocytes of the desert locust (*Schistocerca gregaria*)

revealed that heat-induced chiasma frequency changes are most likely the consequence of the completeness or efficiency of pairing (Henderson, 1988). Thus, we conclude that already very early recombination processes, such as pairing of homologs, are affected by heat and that these aberrant processes likely cause the formation of polycomplexes.

From our mutant analysis and chromosome spreads at elevated temperatures, it is likely that recombination intermediates cause this delay. What the structure of these intermediates is and how they cause a delay needs to be investigated in the future. Possibly, the delay is triggered by nonhomologous recombination caused by mispairing and hence partially interconnected chromosomes. Analysis of a *zmm* mutant in yeast revealed that a specific block in progression of CO formation occurs at high temperatures, resulting in the formation of intermediates and/or interactions with sister chromatids (Borner et al., 2004). Furthermore, it is well known from yeast that unresolved recombination intermediates can cause nuclear division defects (Kaur et al., 2015, 2019; Tang et al., 2015).

Notably, our work also revealed a previously unrecognized delay of the recombination mutants *spo11-1* and *dmc1* in early meiosis of Arabidopsis, that is, in late leptotene/early pachytene, at both high and low temperatures with respect to the WT. A similar extension was clearly seen for *msh4* at HS34°C, with a corresponding tendency for a delay at 21°C. Matching our observations, mutants in *dmc1* in yeast are delayed, too, which was explained by the absence of axial associations between homologs (Rockmill et al., 1995). However, nearly complete synapsis can be detected in *dmc1* mutants in yeast after a substantial delay, while in Arabidopsis *dmc1* mutants stay strictly asynaptic (Couteau et al., 1999). Possibly, this difference is also due to the differently acting pachytene checkpoints in both species (see below).

Another difference between yeast and Arabidopsis concerns *spo11* mutants, which progress faster through prophase I in the yeast mutant than its WT strain, whereas, as shown in this study, Arabidopsis *spo11* mutants are delayed in early prophase in meiosis (Klapholz et al., 1985; Jiao et al., 1999; Cha et al., 2000). The different behavior of these mutants cannot currently be resolved, but possibly hints at different mechanisms of homolog interaction in yeast versus Arabidopsis.

### A specialized pachytene checkpoint in Arabidopsis

Aberrant recombination structures and the absence of recombination trigger an arrest in late prophase I in animals and yeast, executed by the so-called pachytene checkpoint (Bishop et al., 1992; Rockmill et al., 1995; Barchi et al., 2005). Since in plants mutants in which recombination is abolished, such as *dmc1*, are not arrested in meiosis, it has been proposed that plants do not possess a pachytene checkpoint (Couteau et al., 1999; Grelon et al., 2001; Caryl et al., 2003; Higgins et al., 2004; Li et al., 2004, 2009b; Jones and Franklin, 2008).



A major regulator of the pachytene checkpoint in animals and yeast is the checkpoint kinase ATM (Roeder and Bailis, 2000; Barchi et al., 2005; Lange et al., 2011; Pacheco et al., 2015; Penedos et al., 2015). Removing ATM in mutants that trigger the pachytene checkpoint in mice spermatocytes, for instance in weak loss-of-function mutants for Thyroid Hormone Receptor Interactor 13 (also known as Pachytene checkpoint protein homolog 2), restores progression through pachytene, indicating that the early arrest is under control of this checkpoint kinase (Pacheco et al., 2015).

In budding yeast, *atm* mutants undergo the first meiotic division before all recombination events are complete (Lydall et al., 1996; Stuart and Wittenberg, 1998). Correspondingly, we found that the pachytene/diakinesis extension is lost in *Arabidopsis atm* mutants, implicating ATM in this checkpoint and the execution of the observed meiotic delay, for example, by sensing aberrant recombination structures. Together with our finding that the prolongation of pachytene/diakinesis is recombination-dependent, we conclude that *Arabidopsis* and likely other plants do have a pachytene checkpoint. However, this checkpoint appears to be less stringent than in animals, since it does not respond to the absence of meiotic recombination. Moreover, the extension is temporally restricted and typically after 2.7 h meiosis continues. After the nature of the presumptive aberrant recombination intermediates becomes better understood, it should be determined whether they are resolved during this time or whether the checkpoint erodes, that is, meiosis progresses even though checkpoint conditions are not fulfilled. An erosion has been observed for another checkpoint in plants, that is, the spindle assembly checkpoint (SAC), which ensures that all chromosomes are connected to MT fibers of the spindle. Triggering this checkpoint was only able to delay the onset of anaphase by at most <2 h (Komaki and Schnittger, 2017). Notably, the SAC can also erode in mammals and yeast, although typically only after several hours (Rieder and Maiato, 2004; Rossio et al., 2010).

It is an interesting discussion point whether less stringent cell division checkpoints (pachytene and SAC) represent an evolutionary strategy in plants. Genome mutations, especially polyploidization events, are more prominent in plants than in animals and are suspected to be a major driving force of their evolution (Li et al., 2009b; Brownfield and Kohler, 2011; De Storme and Geelen, 2013; Wijnker and Schnittger, 2013). Moreover, hybridization events are very frequent in plants. An alien genome would likely affect recombination by either reducing it or causing aberrant recombination structures. Less stringent checkpoints would pave the road for hybridization events since by chance viable combinations of chromosomes are generated. Especially an interplay between a relaxed pachytene checkpoint and a relaxed SAC may promote rapid genome evolution, as often found in plant species.

## Materials and methods

### Plant materials and growth conditions

All *Arabidopsis* (*A. thaliana*) plants used in this study were in the Columbia-0 accession. The *CDKA1-mVenus TagRFP:TUA5* double reporter line, *KINGBIRD reporter line 2* (*REC8pro:REC8-GFP RPS5Apro:TagRFP-TUA5*) and the *ASY1-RFP ZYP1b-GFP* double reporter line have been previously described (Prusicki et al., 2019; Yang et al., 2019, 2020; Sofroni et al., 2020). Seeds for T-DNA insertion mutants for *DMC1* (GABI\_918E07), *SPO11-1* (SALK\_146172), *MSH4* (SALK\_136296), and *ATM* (SALK\_006953) were obtained from the GABI-Kat T-DNA mutation collection and the collection of T-DNA mutants of the Salk Institute Genomic Analysis Laboratory (<http://signal.salk.edu/cgi-bin/tdnaexpress>) via Nottingham *Arabidopsis* Stock Centre (NASC) (<http://arabidopsis.info/>) (for genotyping primers see Supplemental Table S3).

Seeds were surface sterilized with chlorine gas and germinated on 1% (w/v) agar containing half-strength Murashige and Skoog (MS) salts and 1% (w/v) sucrose, pH 5.8. When required, antibiotics were added for seed selection. All plants were grown under long-day conditions (16 h light at 21°C ( $\pm 0.5^\circ\text{C}$ )/8 h dark at 18°C ( $\pm 0.5^\circ\text{C}$ ), with 60% humidity). For short-term heat treatment, plants were first grown under standard long-day conditions until flowering. Flower buds were then harvested and cultured on agar in petri plates *ex vivo* as previously described (Prusicki et al., 2020). These plates were then exposed to heat shock by transfer to a preheated incubation chamber (30°C or 34°C) mounted on the microscope stage, where meiotic progression was followed in real time.

For the cytology analysis and protein localization studies, plants were transferred to a climate chamber under a long-day photoperiod with constant temperature (30°C/34°C ( $\pm 0.5^\circ\text{C}$ )) for 24/16 h prior to fixation/observation, respectively. For long-term heat treatment, healthy plants at the bolting stage were transferred to a climate chamber under a long-day photoperiod with constant temperature of 30°C ( $\pm 0.5^\circ\text{C}$ ) with 60% humidity for 7 days.

### Plasmids and plant transformation

The reporter constructs *RPS5Apro:TagRFP-TUA5* and *KINGBIRD reporter line 2*, previously described (Prusicki et al., 2019), were transformed into the T-DNA insertion mutants by floral dipping. T<sub>1</sub> seeds were selected on half-strength MS medium containing the antibiotic hygromycin. All observations were carried out with T<sub>2</sub> lines.

### Confocal microscopy and intensity plots

For protein localization experiments, healthy flower buds were dissected exposing two anthers and carefully positioned in a petri plate filled with half-strength MS medium, pH 5.8 solidified with 0.8% (w/v) agar, and meiocytes of different meiotic stages were imaged using a Zeiss LSM880 confocal microscope.

For pixel intensity plots, flower buds were dissected and the anthers in MT array state 6 were imaged using a Zeiss LSM880 confocal microscope with the exact same settings for the different heat conditions. The pixel brightness was measured through a region of interest using ImageJ (Schindelin et al., 2012; Schneider et al., 2012) and plotted against the X dimension, which is the distance of the region of interest.

### Live cell imaging and data processing

Live cell imaging was performed as described previously (Prusicki et al., 2019). In short, up to six flower buds of 0.2–0.6 mm were carefully positioned in a petri plate filled with half-strength MS medium, pH 5.8 and solidified with 0.8% (w/v) agar. Time lapse was performed using an upright Zeiss LSM 880 confocal microscope with ZEN 2.3 SP1 software (Carl Zeiss AG, Oberkochen, Germany) and a W-plan Apochromat 40X/1.0 DIC objective (Carl Zeiss AG, Oberkochen, Germany). GFP and TagRFP were excited at  $\lambda = 488$  nm and 561 nm, respectively, and detected between 498 and 560 nm and 520 and 650 nm, respectively. Auto-fluorescence was detected between 680 and 750 nm. With a time interval of 10 min, a series of six Z-stacks with 50  $\mu$ m distance was acquired under a thermally controlled environment (21°C/30°C/34°C [ $\pm$  0.15%]) in an incubation chamber. Due to sample movement, the Z-planes were manually selected using the review multi-dimensional data function of the software Metamorph version 7.8 and the XY movement was corrected using the Stack Reg plugin of Fiji.

### Quantitative analysis of the meiotic phases

The analysis of the duration was based on the *TagRFP-TUA5* reporter. Meiocytes were manually assigned to defined MT states (Supplemental Data Sets S1 and S2). The data were collected from a minimum of three independent set-ups, with a minimum of eight anthers per genotype per heat treatment. The durations of the meiotic phases were extracted from at least 65 meiocytes.

### Statistical methods

Parametric models for interval-censored survival time data with a clustered sandwich estimator of variance were applied to address the clustering of meiocytes within anthers, including effects of the heat treatment, genotype, and their interaction. The underlying distribution of the parametric model was chosen based on the Akaike Information Criterion with exponential, Gompertz, log-logistic, Weibull, and log-normal distribution as candidates.

The models used information from all cells for which we observed at least one time point in the respective state. The event of interest is the transition of a cell from one state to the next. Each cell for which the exact beginning and end of the state were known was modeled as having an event, with the event time calculated as the difference between the start of the next state and the end of the previous state. Cells, where the exact time points of either the transition from the previous state to the state of interest or to the

next state were not known, were modeled as interval-censored data points, with the lower limit of the interval being the time where the cell was observed in this specific state and the upper limit of the interval being one time unit after/before the cell was observed in the previous/next state, respectively. If for a cell the state before or after the current state of interest was not observed at all, the cell was modeled as right-censored with the censoring time being the maximum observed time (i.e. the minimum actual time in this state) for this cell in the state of interest. In addition to the individual states, we also calculated a model for the duration from MT array states 2–13 in an analogous fashion. In specific models, some combinations of heat treatment and genotype had to be excluded because no (or hardly any) events were observed.

The chosen distributions underlying our parametric model were log-normal for MT array states 7–8–9, 10–11, 12–13, 14, while a Weibull distribution was selected for MT array states 2–3–4 and 5–6 and the model for the complete duration of MT array states 2–13. Estimation results are presented as predicted marginal median times (or corresponding contrasts), together with 95% CIs. Since the analysis is of an exploratory nature, no adjustment for multiplicity was applied. The statistical analysis was performed with R version 3.5.1 and Stata SE version 16.1.

Scripts are available at [https://github.com/linda-kr/Heatstress\\_Meiosis](https://github.com/linda-kr/Heatstress_Meiosis).

### Cytology

The cytological analysis of the meiocytes under short and long heat treatment was conducted by performing chromosome spreads, as previously described (Sofroni et al., 2020). Briefly, healthy flower buds were fixed in ethanol:acetic acid (3:1, v/v) for a minimum of 24 h at 4°C, following washing steps with 70% (v/v) ethanol, and stored at 4°C. Next, flower buds were washed in water and in 10 mM citrate buffer, pH 4.5 and digested in an enzyme mix (10 mM citrate buffer containing 0.5% [w/v] cellulase, 0.5% [w/v] pectolyase, and 0.5% [w/v] cytohelicase) for 2.5 h at 37°C. Digested flower buds were squashed and spread onto a glass slide in 45% (v/v) acetic acid on a 46°C hot plate. Finally, the slides were washed in cold ethanol:acetic acid (3:1, v/v) and mounted in Vectashield medium with 4',6-diamidino-2-phenylindole (Vector Laboratories, San Francisco, CA, USA).

### Accession numbers

Accession numbers based on The Arabidopsis Information Resource (<https://www.arabidopsis.org>) for all genes examined in this study are *DMC1* (At3g22880), *SPO11-1* (At3g13170), *MSH4* (At4g1738), and *ATM* (At3g48190).

### Supplemental data

The following materials are available in the online version of this article.

**Supplemental Figure S1.** MT array states upon heat stress.

**Supplemental Figure S2.** Meiotic defects of the WT upon heat stress.

**Supplemental Figure S3.** Duration of meiotic phases in recombination mutants *spo11-1*, *dmc1*, *msh4*, and *atm* at 21°C and HS34°C.

**Supplemental Table S1.** Detailed overview of the sample sizes.

**Supplemental Table S2.** Pairwise comparisons of the meiotic phases.

**Supplemental Table S3.** Genotyping primers.

**Supplemental Movie S1.** Meiotic division of *spo11-1* meiocytes at 21°C.

**Supplemental Movie S2.** Meiotic division of *dmc1* meiocytes at 21°C.

**Supplemental Movie S3.** Meiotic division of *msh4* meiocytes at 21°C.

**Supplemental Movie S4.** Meiotic division of *spo11-1* meiocytes at HS34°C.

**Supplemental Movie S5.** Meiotic division of *dmc1* meiocytes at HS34°C.

**Supplemental Movie S6.** Meiotic division of *msh4* meiocytes at HS34°C.

**Supplemental Movie S7.** Meiotic division of *atm* meiocytes at 21°C.

**Supplemental Movie S8.** Meiotic division of *atm* meiocytes at HS34°C.

**Supplemental Data Set S1.** Raw data imaging for WT.

**Supplemental Data Set S2.** Raw data imaging for the mutants.

## Acknowledgments

We thank Lucas Lang (University of Hamburg) and Konstantinos Lampou (University of Hamburg) for critical reading and helpful comments on the manuscript. We are grateful to Chao Yang, Shinichiro Komaki, and Konstantinos Lampou for providing the reporter lines in the mutant background.

## Funding

This research was funded by the University of Hamburg.

**Conflict of interest statement.** None declared.

## References

- Anderson P, Kedersha N (2002) Visibly stressed: the role of eIF2, TIA-1, and stress granules in protein translation. *Cell Stress Chaperones* **7**: 13–221
- Anderson P, Kedersha N (2008) Stress granules: the Tao of RNA triage. *Trends Biochem Sci* **33**: 141–150
- Anderson TR, Hawkins E, Jones PD (2016) CO<sub>2</sub>, the greenhouse effect and global warming: from the pioneering work of Arrhenius and Callendar to today's Earth System Models. *Endeavour* **40**: 178–187
- Armstrong SJ, Caryl AP, Jones GH, Franklin FC (2002) Asy1, a protein required for meiotic chromosome synapsis, localizes to axis-associated chromatin in *Arabidopsis* and *Brassica*. *J Cell Sci* **115**: 3645–3655
- Armstrong SJ, Franklin FCH, Jones GH (2003) A meiotic time-course for *Arabidopsis thaliana*. *Sex Plant Reprod* **16**: 141–149
- Bannigan A, Scheible WR, Lukowitz W, Fagerstrom C, Wadsworth P, Somerville C, Baskin TI (2007) A conserved role for kinesin-5 in plant mitosis. *J Cell Sci* **120**: 2819–2827
- Barchi M, Mahadevaiah S, Di Giacomo M, Baudat F, de Rooij DG, Burgoyne PS, Jasin M, Keeney S (2005) Surveillance of different recombination defects in mouse spermatocytes yields distinct responses despite elimination at an identical developmental stage. *Mol Cell Biol* **25**: 7203–7215
- Bennett MD, Smith JB, Kemble R (1972) The effect of temperature on meiosis and pollen development in wheat and rye. *Can J Genet Cytol* **14**: 615–624
- Berchowitz LE, Francis KE, Bey AL, Copenhaver GP (2007) The role of AtMUS81 in interference-insensitive crossovers in *A. thaliana*. *PLoS Genet* **3**: e132
- Bilgic C, Dombecki CR, Chen PF, Villeneuve AM, Nabeshima K (2013) Assembly of the synaptonemal complex is a highly temperature-sensitive process that is supported by PGL-1 during *Caenorhabditis elegans* meiosis. *G3 (Bethesda)* **3**: 585–595
- Bishop DK, Park D, Xu L, Kleckner N (1992) DMC1: a meiosis-specific yeast homolog of E. coli recA required for recombination, synaptonemal complex formation, and cell cycle progression. *Cell* **69**: 439–456
- Bomblies K, Higgins JD, Yant L (2015) Meiosis evolves: adaptation to external and internal environments. *New Phytol* **208**: 306–323
- Borner GV, Kleckner N, Hunter N (2004) Crossover/noncrossover differentiation, synaptonemal complex formation, and regulatory surveillance at the leptotene/zygotene transition of meiosis. *Cell* **117**: 29–45
- Brar GA, Kiburz BM, Zhang Y, Kim JE, White F, Amon A (2006) Rec8 phosphorylation and recombination promote the step-wise loss of cohesins in meiosis. *Nature* **441**: 532–536
- Brar GA, Yassour M, Friedman N, Regev A, Ingolia NT, Weissman JS (2012) High-resolution view of the yeast meiotic program revealed by ribosome profiling. *Science* **335**: 552–557
- Brown SD, Audouyoud C, Lorenz A (2020) Intragenic meiotic recombination in *Schizosaccharomyces pombe* is sensitive to environmental temperature changes. *Chromosome Res* **28**: 195–207
- Brownfield L, Kohler C (2011) Unreduced gamete formation in plants: mechanisms and prospects. *J Exp Bot* **62**: 1659–1668
- Buchan JR, Parker R (2009) Eukaryotic stress granules: the ins and outs of translation. *Mol Cell* **36**: 932–941
- Bulankova P, Riehs-Kearnan N, Nowack MK, Schnittger A, Riha K (2010) Meiotic progression in *Arabidopsis* is governed by complex regulatory interactions between SMG7, TDM1, and the meiosis I-specific cyclin TAM. *Plant Cell* **22**: 3791–3803
- Cai X, Dong F, Edelmann RE, Makaroff CA (2003) The *Arabidopsis* SYN1 cohesin protein is required for sister chromatid arm cohesion and homologous chromosome pairing. *J Cell Sci* **116**: 2999–3007
- Capilla-Perez L, Durand S, Hurel A, Lian Q, Chambon A, Taohy C, Solier V, Grelon M, Mercier R (2021) The synaptonemal complex imposes crossover interference and heterochiasmy in *Arabidopsis*. *Proc Natl Acad Sci USA* **118**: e2023613118
- Caryl AP, Armstrong SJ, Jones GH, Franklin FC (2000) A homologue of the yeast HOP1 gene is inactivated in the *Arabidopsis* meiotic mutant *asy1*. *Chromosoma* **109**: 62–71
- Caryl AP, Jones GH, Franklin FC (2003) Dissecting plant meiosis using *Arabidopsis thaliana* mutants. *J Exp Bot* **54**: 25–38
- Cha RS, Weiner BM, Keeney S, Dekker J, Kleckner N (2000) Progression of meiotic DNA replication is modulated by interchromosomal interaction proteins, negatively by Spo11p and positively by Rec8p. *Genes Dev* **14**: 493–503
- Chodasiewicz M, Sokolowska EM, Nelson-Dittrich AC, Masiuk A, Beltran JCM, Nelson ADL, Skirycz A (2020) Identification and characterization of the heat-induced plastidial stress granules reveal new insight into *Arabidopsis* stress response. *Front Plant Sci* **11**: 595792



- Ciska M, Moreno Diaz de la Espina S (2013) NMCP/LINC proteins: putative lamin analogs in plants? *Plant Signal Behav* **8**: e26669
- Collins M (2014) Long-term climate change: projections, commitments and irreversibility pages 1029 to 1076. In *Intergovernmental Panel on Climate Change, ed, Climate Change 2013–The Physical Science Basis: Working Group I Contribution to the Fifth Assessment Report of the Intergovernmental Panel on Climate Change*, Cambridge University Press, Cambridge, pp 1029–1136
- Couteau F, Belzile F, Horlow C, Grandjean O, Vezon D, Doutriaux MP (1999) Random chromosome segregation without meiotic arrest in both male and female meiocytes of a *dmc1* mutant of *Arabidopsis*. *Plant Cell* **11**: 1623–1634
- Crichton JH, Read D, Adams IR (2018) Defects in meiotic recombination delay progression through pachytene in *Tex19.1(-/-)* mouse spermatocytes. *Chromosoma* **127**: 437–459
- de Rooij DG, de Boer P (2003) Specific arrests of spermatogenesis in genetically modified and mutant mice. *Cytogenet Genome Res* **103**: 267–276
- De Storme N, Geelen D (2013) Sexual polyploidization in plants—cytological mechanisms and molecular regulation. *New Phytol* **198**: 670–684
- De Storme N, Geelen D (2020) High temperatures alter cross-over distribution and induce male meiotic restitution in *Arabidopsis thaliana*. *Commun Biol* **3**: 187
- Dissmeyer N, Nowack MK, Pusch S, Stals H, Inze D, Grini PE, Schnittger A (2007) T-loop phosphorylation of *Arabidopsis* CDKA; 1 is required for its function and can be partially substituted by an aspartate residue. *Plant Cell* **19**: 972–985
- Dowrick GJ (1957) The influence of temperature on meiosis. *Heredity* **11**: 37–49
- Draeger T, Moore G (2017) Short periods of high temperature during meiosis prevent normal meiotic progression and reduce grain number in hexaploid wheat (*Triticum aestivum* L.). *Theor Appl Genet* **130**: 1785–1800
- Dubiel M, De Coninck T, Osterne VJS, Verbeke I, Van Damme D, Smaghe G, Van Damme EJM (2020) The ArathEULS3 lectin ends up in stress granules and can follow an unconventional route for secretion. *Int J Mol Sci* **21**: 1659
- Fiserova J, Goldberg MW (2010) Relationships at the nuclear envelope: lamins and nuclear pore complexes in animals and plants. *Biochem Soc Trans* **38**: 829–831
- France MG, Enderle J, Rohrig S, Puchta H, Franklin FCH, Higgins JD (2021) ZYP1 is required for obligate cross-over formation and cross-over interference in *Arabidopsis*. *Proc Natl Acad Sci USA* **118**: e2021671118
- Garcia V, Bruchet H, Camescasse D, Granier F, Bouchez D, Tissier A (2003) AtATM is essential for meiosis and the somatic response to DNA damage in plants. *Plant Cell* **15**: 119–132
- Grelon M, Vezon D, Gendrot G, Pelletier G (2001) AtSPO11-1 is necessary for efficient meiotic recombination in plants. *EMBO J* **20**: 589–600
- Hamada T, Yako M, Minegishi M, Sato M, Kamei Y, Yanagawa Y, Toyooka K, Watanabe Y, Hara-Nishimura I (2018) Stress granule formation is induced by a threshold temperature rather than a temperature difference in *Arabidopsis*. *J Cell Sci* **131**: jcs216051
- Hartung F, Wurz-Wildersinn R, Fuchs J, Schubert I, Suer S, Puchta H (2007) The catalytically active tyrosine residues of both SPO11-1 and SPO11-2 are required for meiotic double-strand break induction in *Arabidopsis*. *Plant Cell* **19**: 3090–3099
- Hatfield JL, Prueger JH (2015) Temperature extremes: effect on plant growth and development. *Weather Clim Extremes* **10**: 4–10
- Hedhly A, Nestorova A, Herrmann A, Grossniklaus U (2020) Acute heat stress during stamen development affects both the germline and sporophytic lineages in *Arabidopsis thaliana* (L.) Heynh. *Environ Exp Bot* **173**: 103992
- Henderson SA (1988) Four effects of elevated temperature on chiasma formation in the locust *Schistocerca gregaria*. *Heredity* **60**: 387–401
- Higgins JD, Armstrong SJ, Franklin FC, Jones GH (2004) The *Arabidopsis* MutS homolog AtMSH4 functions at an early step in recombination: evidence for two classes of recombination in *Arabidopsis*. *Genes Dev* **18**: 2557–2570
- Higgins JD, Perry RM, Barakate A, Ramsay L, Waugh R, Halpin C, Armstrong SJ, Franklin FC (2012) Spatiotemporal asymmetry of the meiotic program underlies the predominantly distal distribution of meiotic crossovers in barley. *Plant Cell* **24**: 4096–4109
- Higgins JD, Sanchez-Moran E, Armstrong SJ, Jones GH, Franklin FC (2005) The *Arabidopsis* synaptonemal complex protein ZYP1 is required for chromosome synapsis and normal fidelity of crossing over. *Genes Dev* **19**: 2488–2500
- Interthal H, Heyer WD (2000) MUS81 encodes a novel helix-hairpin-helix protein involved in the response to UV- and methylation-induced DNA damage in *Saccharomyces cerevisiae*. *Mol Gen Genet* **263**: 812–827
- Jachymczyk WJ, von Borstel RC, Mowat MR, Hastings PJ (1981) Repair of interstrand cross-links in DNA of *Saccharomyces cerevisiae* requires two systems for DNA repair: the RAD3 system and the RAD51 system. *Mol Gen Genet* **182**: 196–205
- Jiao K, Bullard SA, Salem L, Malone RE (1999) Coordination of the initiation of recombination and the reductional division in meiosis in *Saccharomyces cerevisiae*. *Genetics* **152**: 117–128
- Jones GH, Franklin FCH (2008) Meiosis in *Arabidopsis thaliana*: recombination, chromosome organization and meiotic progression. In R Egel, DH Lankenau, eds, *Recombination and Meiosis: Crossing-Over and Disjunction*, Springer Berlin Heidelberg, Berlin, Heidelberg, Germany, pp 279–306
- Kaur H, De Muyt A, Lichten M (2015) Top3-Rmi1 DNA single-strand decatenase is integral to the formation and resolution of meiotic recombination intermediates. *Mol Cell* **57**: 583–594
- Kaur H, Gn K, Lichten M (2019) Unresolved recombination intermediates cause a RAD9-dependent cell cycle arrest in *Saccharomyces cerevisiae*. *Genetics* **213**: 805–818
- Keeney S, Giroux CN, Kleckner N (1997) Meiosis-specific DNA double-strand breaks are catalyzed by Spo11, a member of a widely conserved protein family. *Cell* **88**: 375–384
- Kim B, Cooke HJ, Rhee K (2012) DAZL is essential for stress granule formation implicated in germ cell survival upon heat stress. *Development* **139**: 568–578
- Klapholz S, Waddell CS, Esposito RE (1985) The role of the SPO11 gene in meiotic recombination in yeast. *Genetics* **110**: 187–216
- Komaki S, Schnittger A (2017) The spindle assembly checkpoint in *Arabidopsis* is rapidly shut off during severe stress. *Dev Cell* **43**: 172–185 e175
- Kosmacz M, Gorka M, Schmidt S, Luzarowski M, Moreno JC, Szlachetko J, Leniak E, Sokolowska EM, Sofroni K, Schnittger A, et al. (2019) Protein and metabolite composition of *Arabidopsis* stress granules. *New Phytol* **222**: 1420–1433
- Kukul MS, Irmak S (2018) Climate-driven crop yield and yield variability and climate change impacts on the U.S. great plains agricultural production. *Sci Rep* **8**: 3450
- Kurzbaue MT, Janisiw MP, Paulin LF, Prusen Mota I, Tomanov K, Krsicka O, Haeseler AV, Schubert V, Schlogelhofer P (2021) ATM controls meiotic DNA double-strand break formation and recombination and affects synaptonemal complex organization in plants. *Plant Cell* **33**: 1633–1656
- Kurzbaue MT, Uanschou C, Chen D, Schlogelhofer P (2012) The recombinases DMC1 and RAD51 are functionally and spatially separated during meiosis in *Arabidopsis*. *Plant Cell* **24**: 2058–2070
- Lamb BC (1969) Related and unrelated changes in conversion and recombination frequencies with temperature in *Sordaria fimicola*, and their relevance to hybrid-DNA models of recombination. *Genetics* **62**: 67–78
- Lange J, Pan J, Cole F, Thelen MP, Jasin M, Keeney S (2011) ATM controls meiotic double-strand-break formation. *Nature* **479**: 237–240

- Lee YJ, Liu B (2019) Microtubule nucleation for the assembly of acentrosomal microtubule arrays in plant cells. *New Phytol* **222**: 1705–1718
- Lei X, Ning Y, Eid Elesawi I, Yang K, Chen C, Wang C, Liu B (2020) Heat stress interferes with chromosome segregation and cytokinesis during male meiosis in *Arabidopsis thaliana*. *Plant Signal Behav* **15**: 1746985
- Li H, Zeng X, Liu ZQ, Meng QT, Yuan M, Mao TL (2009a) Arabidopsis microtubule-associated protein AtMAP65-2 acts as a microtubule stabilizer. *Plant Mol Biol* **69**: 313–324
- Li W, Chen C, Markmann-Mulisch U, Timofejeva L, Schmelzer E, Ma H, Reiss B (2004) The Arabidopsis AtRAD51 gene is dispensable for vegetative development but required for meiosis. *Proc Natl Acad Sci USA* **101**: 10596–10601
- Li XC, Barringer BC, Barbash DA (2009b) The pachytene checkpoint and its relationship to evolutionary patterns of polyploidization and hybrid sterility. *Heredity (Edinb)* **102**: 24–30
- Liu B, De Storme N, Geelen D (2017) Cold interferes with male meiotic cytokinesis in *Arabidopsis thaliana* independently of the AHK2/3-AHP2/3/5 cytokinin signaling module. *Cell Biol Int* **41**: 879–889
- Lloyd A, Morgan C, FC HFBomblyes K (2018) Plasticity of meiotic recombination rates in response to temperature in *Arabidopsis*. *Genetics* **208**: 1409–1420
- Loidl J (1989) Effects of elevated temperature on meiotic chromosome synapsis in *Allium ursinum*. *Chromosoma* **97**: 449–458
- Lydall D, Nikolsky Y, Bishop DK, Weinert T (1996) A meiotic recombination checkpoint controlled by mitotic checkpoint genes. *Nature* **383**: 840–843
- Modliszewski JL, Wang H, Albright AR, Lewis SM, Bennett AR, Huang J, Ma H, Wang Y, Copenhaver GP (2018) Elevated temperature increases meiotic crossover frequency via the interfering (Type I) pathway in *Arabidopsis thaliana*. *PLoS Genet* **14**: e1007384
- Morgan CH, Zhang H, Bomblyes K (2017) Are the effects of elevated temperature on meiotic recombination and thermotolerance linked via the axis and synaptonemal complex? *Philos Trans R Soc Lond B Biol Sci* **372**: 20160470
- Nebel BR, Hackett EM (1961) Synaptonemal complexes (cores) in primary spermatocytes of mouse under elevated temperature. *Nature* **190**: 467–468
- Osman K, Sanchez-Moran E, Higgins JD, Jones GH, Franklin FC (2006) Chromosome synapsis in *Arabidopsis*: analysis of the transverse filament protein ZYP1 reveals novel functions for the synaptonemal complex. *Chromosoma* **115**: 212–219
- Pacheco S, Marcet-Ortega M, Lange J, Jasin M, Keeney S, Roig I (2015) The ATM signaling cascade promotes recombination-dependent pachytene arrest in mouse spermatocytes. *PLoS Genet* **11**: e1005017
- Pao WK, Li HW (1948) Desynapsis and other abnormalities induced by high temperature. *J Genet* **48**: 297–310
- Pecrix Y, Rallo G, Folzer H, Cigna M, Gudin S, Le Bris M (2011) Polyploidization mechanisms: temperature environment can induce diploid gamete formation in *Rosa* sp. *J Exp Bot* **62**: 3587–3597
- Penedos A, Johnson AL, Strong E, Goldman AS, Carballo JA, Cha RS (2015) Essential and checkpoint functions of budding yeast ATM and ATR during meiotic prophase are facilitated by differential phosphorylation of a meiotic adaptor protein, Hop1. *PLoS One* **10**: e0134297
- Phillips D, Jenkins G, Macaulay M, Nibau C, Wnetrzak J, Fallding D, Colas I, Oakey H, Waugh R, Ramsay L (2015) The effect of temperature on the male and female recombination landscape of barley. *New Phytol* **208**: 421–429
- Prusicki MA, Hamamura Y, Schnittger A (2020) A practical guide to live-cell imaging of meiosis in *Arabidopsis*. *Methods Mol Biol* **2061**: 3–12
- Prusicki MA, Keizer EM, van Rosmalen RP, Komaki S, Seifert F, Muller K, Wijnker E, Fleck C, Schnittger A (2019) Live cell imaging of meiosis in *Arabidopsis thaliana*. *Elife* **8**: e42834
- Pusch S, Dissmeyer N, Schnittger A (2011) Bimolecular-fluorescence complementation assay to monitor kinase-substrate interactions in vivo. *Methods Mol Biol* **779**: 245–257
- Rieder CL, Maiato H (2004) Stuck in division or passing through: what happens when cells cannot satisfy the spindle assembly checkpoint. *Dev Cell* **7**: 637–651
- Rockmill B, Sym M, Scherthan H, Roeder GS (1995) Roles for two RecA homologs in promoting meiotic chromosome synapsis. *Genes Dev* **9**: 2684–2695
- Roeder GS, Bailis JM (2000) The pachytene checkpoint. *Trends Genet* **16**: 395–403
- Rossio V, Galati E, Piatti S (2010) Adapt or die: how eukaryotic cells respond to prolonged activation of the spindle assembly checkpoint. *Biochem Soc Trans* **38**: 1645–1649
- Sanchez-Moran E, Santos JL, Jones GH, Franklin FC (2007) ASY1 mediates AtDMC1-dependent interhomolog recombination during meiosis in *Arabidopsis*. *Genes Dev* **21**: 2220–2233
- Santucci-Darmanin S, Neyton S, Lespinasse F, Saunieres A, Gaudray P, Paquis-Flucklinger V (2002) The DNA mismatch-repair MLH3 protein interacts with MSH4 in meiotic cells, supporting a role for this MutL homolog in mammalian meiotic recombination. *Hum Mol Genet* **11**: 1697–1706
- Schindelin J, Arganda-Carreras I, Frise E, Kaynig V, Longair M, Pietzsch T, Preibisch S, Rueden C, Saalfeld S, Schmid B, et al. (2012) Fiji: an open-source platform for biological-image analysis. *Nat Methods* **9**: 676–682
- Schneider CA, Rasband WS, Eliceiri KW (2012) NIH Image to ImageJ: 25 years of image analysis. *Nat Methods* **9**: 671–675
- Sofroni K, Takatsuka H, Yang C, Dissmeyer N, Komaki S, Hamamura Y, Bottger L, Umeda M, Schnittger A (2020) CDK-dependent activation of CDKA1 controls microtubule dynamics and cytokinesis during meiosis. *J Cell Biol* **219**: e201907016
- Song P, Jia Q, Chen L, Jin X, Xiao X, Li L, Chen H, Qu Y, Su Y, Zhang W, et al. (2020) Involvement of *Arabidopsis* phospholipase D delta in regulation of ROS-mediated microtubule organization and stomatal movement upon heat shock. *J Exp Bot* **71**: 6555–6570
- Stacey NJ, Kuromori T, Azumi Y, Roberts G, Breuer C, Wada T, Maxwell A, Roberts K, Sugimoto-Shirasu K (2006) *Arabidopsis* SPO11-2 functions with SPO11-1 in meiotic recombination. *Plant J* **48**: 206–216
- Stefani A, Colonna N (1996) The influence of temperature on meiosis and microspores development in *Dasyphyllum villosum* (L.) P. Candargy. *Cytologia* **61**: 277–283
- Stronghill PE, Azimi W, Hasenkampf CA (2014) A novel method to follow meiotic progression in *Arabidopsis* using confocal microscopy and 5-ethynyl-2'-deoxyuridine labeling. *Plant Methods* **10**: 33
- Stuart D, Wittenberg C (1998) CLB5 and CLB6 are required for pre-meiotic DNA replication and activation of the meiotic S/M checkpoint. *Genes Dev* **12**: 2698–2710
- Su SS, Modrich P (1986) *Escherichia coli* mutS-encoded protein binds to mismatched DNA base pairs. *Proc Natl Acad Sci USA* **83**: 5057–5061
- Tang S, Wu MKY, Zhang R, Hunter N (2015) Pervasive and essential roles of the Top3-Rmi1 decatenase orchestrate recombination and facilitate chromosome segregation in meiosis. *Mol Cell* **57**: 607–621
- Toca-Herrera JL, Kupcu S, Diederichs V, Moncayo G, Pum D, Sleytr UB (2006) Fluorescence emission properties of S-Layer enhanced green fluorescent fusion protein as a function of temperature, pH conditions, and guanidine hydrochloride concentration. *Biomacromolecules* **7**: 3298–3301
- Wang J, Li D, Shang F, Kang X (2017) High temperature-induced production of unreduced pollen and its cytological effects in *Populus*. *Sci Rep* **7**: 5281
- Wijnker E, Harashima H, Muller K, Parra-Nunez P, de Snoo CB, van de Belt J, Dissmeyer N, Bayer M, Pradillo M, Schnittger A (2019) The Cdk1/Cdk2 homolog CDKA1 controls the

- recombination landscape in *Arabidopsis*. *Proc Natl Acad Sci USA* **116**: 12534–12539
- Wijnker E, Schnittger A** (2013) Control of the meiotic cell division program in plants. *Plant Reprod* **26**: 143–158
- Wilson JY** (1959) Duration of meiosis in relation to temperature. *Heredity* **13**: 263–267
- Wu S, Scheible WR, Schindelasch D, Van Den Daele H, De Veylder L, Baskin TI** (2010) A conditional mutation in *Arabidopsis thaliana* separase induces chromosome non-disjunction, aberrant morphogenesis and cyclin B1;1 stability. *Development* **137**: 953–961
- Yahya G, Perez AP, Mendoza MB, Parisi E, Moreno DF, Artes MH, Gallego C, Aldea M** (2021) Stress granules display bistable dynamics modulated by Cdk. *J Cell Biol* **220**: e202005102
- Yang C, Hamamura Y, Sofroni K, Bower F, Stolze SC, Nakagami H, Schnittger A** (2019) SWITCH 1/DYAD is a WINGS APART-LIKE antagonist that maintains sister chromatid cohesion in meiosis. *Nat Commun* **10**: 1755
- Yang C, Sofroni K, Wijnker E, Hamamura Y, Carstens L, Harashima H, Stolze SC, Vezon D, Chelysheva L, Orban-Nemeth Z, et al.** (2020) The *Arabidopsis* Cdk1/Cdk2 homolog CDKA;1 controls chromosome axis assembly during plant meiosis. *EMBO J* **39**: e101625
- Yao Y, Li X, Chen W, Liu H, Mi L, Ren D, Mo A, Lu P** (2020) ATM promotes RAD51-mediated meiotic DSB repair by inter-sister-chromatid recombination in *Arabidopsis*. *Front Plant Sci* **11**: 839
- Yue Y, Zhang P, Shang Y** (2019) The potential global distribution and dynamics of wheat under multiple climate change scenarios. *Sci Total Environ* **688**: 1308–1318
- Zhao X, Bramsiepe J, Van Durme M, Komaki S, Prusicki MA, Maruyama D, Forner J, Medzihradszky A, Wijnker E, Harashima H, et al.** (2017) RETINOBLASTOMA RELATED1 mediates germline entry in *Arabidopsis*. *Science* **356**: eaaf6532
- Zhao X, Harashima H, Dissmeyer N, Pusch S, Weimer AK, Bramsiepe J, Bouyer D, Rademacher S, Nowack MK, Novak B, et al.** (2012) A general G1/S-phase cell-cycle control module in the flowering plant *Arabidopsis thaliana*. *PLoS Genet* **8**: e1002847